Gravitational Waves from Merging Compact Binaries

Scott A. Hughes

Department of Physics and MIT Kavli Institute, Massachusetts Institute of Technology,
Cambridge, Massachusetts 02139; email: sahughes@mit.edu

Key Words

compact objects, relativistic binaries

Abstract

Largely motivated by the development of highly sensitive gravitational-wave
detectors, our understanding of merging compact binaries and the gravita-
tional waves they generate has improved dramatically in recent years. Break-
throughs in numerical relativity now allow us to model the coalescence of two
black holes with no approximations or simplifications. There has also been
outstanding progress in our analytical understanding of binaries. We review
these developments, examining merging binaries using black hole perturba-
tion theory, post-Newtonian expansions, and direct numerical integration
of the field equations. We summarize these approaches and what they have
taught us about gravitational waves from compact binaries. We place these
results in the context of gravitational-wave generating systems, analyzing
the impact gravitational-wave emission has on their sources, as well as what
we can learn about them from direct gravitational-wave measurements.

1. INTRODUCTION

1.1. History and Motivation

Most physics students learn to solve the Newtonian gravitational two-body problem early in their studies. An exact solution for point masses requires only a few equations and an elliptic integral. Coupling this simple solution to perturbation theory lets us include the effect of nonspherical mass distributions and the impact of additional bodies. We can then accurately model an enormous range of astrophysically interesting and important systems.

By contrast, no exact analytic solution describes binaries in general relativity (GR). GR is nonlinear (making analytic solutions difficult to find except for problems that are highly symmetric) and includes radiation (so that any bound solution will evolve as waves carry off energy and angular momentum). Indeed, for systems containing black holes, GR doesn't so much have a "two-body" problem as it has a "one-spacetime" problem: One cannot even delineate where the boundaries (the event horizons) of the "bodies" are until the entire spacetime describing the binary has been constructed.

Such difficulties in describing binary systems in GR bedeviled the theoretical development of this topic. Many early discussions centered on the even more fundamental question of which motions would generate radiation and which would not. A particularly clear formulation of the confusion is expressed in attempts to answer the following question: If a charge falls freely in the Earth's gravitational field, does it radiate? On one hand, in this nonrelativistic limit, we should expect that our usual intuition regarding accelerating charges would hold, and a falling charge should radiate exactly as described by Jackson (1975) with an acceleration $\vec{a} = -g\vec{e}_r$. On the other hand, in GR a falling charge simply follows a geodesic of the Earth's curved spacetime; it is not "accelerating" relative to freely falling frames, and so is not accelerating in a meaningful sense. The charge just follows the trajectory geometry demands it follows. In this picture, the falling charge appears not to radiate. John Wheeler once asked a group of relativity theorists to vote on whether the falling charge radiates or not; their responses were split almost precisely down the middle (Kennefick 2007, p. 157). (See the sidebar, Radiation from a Falling Charge.)

Similar conceptual issues affect the general two-body problem in relativity. As recently as 1976, Ehlers and colleagues (1976) pointed out that there had not yet been a fully self-consistent derivation for the energy loss from a binary due to gravitational-wave (GW) backreaction. A major motivation for this criticism was the discovery of the binary pulsar PSR 1913+16 (Hulse & Taylor 1975). It was clear that this system would be a powerful laboratory for testing theories of gravity, including the role of GW emission. However, as Ehlers et al. noted, the theoretical framework needed for such tests was not in good shape. Various approaches to understanding the evolution of binary systems tended to be inconsistent in the nature of the approximations they made, often treating the motion of the members of the binary at a different level of rigor than they treated

RADIATION FROM A FALLING CHARGE

What actually happens to a falling charge is now understood thanks to work by Dewitt & Brehme (1960): The charge does radiate, precisely reproducing the nonrelativistic limit. The intuition that it follows a geodesic is not quite right. Though the charge "wants" to follow a geodesic, the charge plus its associated field is extended and nonlocal, and so cannot follow a geodesic. The bending of the charge's field as it falls in spacetime enforces the laws of radiation emission.

the solution for the spacetime. These discrepancies were most notable when the members of the binary were strongly self-gravitating; a weak-field approach is ill-suited to a binary containing neutron stars or black holes. These calculations generally predicted that the system would, at leading order, lose energy at a rate related to the third time derivative of the source's "quadrupole moment." However, the precise definition of this moment for strong-field sources was not always clear.

The Ehlers et al. criticism served as a wake-up call, motivating the formulation of methods for modeling binary dynamics in a mathematically rigorous and self-consistent manner. Several independent approaches were developed; a concise and cogent summary of the principles and the leading results is given by Damour (1983b). For the purpose of this review, a major lesson of the theoretical developments from this body of work is that the so-called quadrupole formula describing the loss of orbital energy and angular momentum owing to GW emission is valid. Somewhat amazingly, one finds that the equations of motion are insensitive to much of the detailed structure of a binary's members. Features such as the members' size and compactness can be absorbed into the definition of their masses. This "principle of effacement" (Damour 1983a) tells us that the motions of two bodies with masses m_1 and m_2 can be predicted independent of whether those bodies are stars, neutron stars, or black holes. [Other aspects of the members' structure cannot be so simply absorbed by the principle of effacement. For example, at a certain order, the spins of a binary's members impact its motion. Spin's effects cannot be absorbed into the definition of mass, but affect the binary's dynamics directly. See Thorne & Hartle (1985) for further detailed discussion.] Over 30 years of observations have since found extraordinary agreement between prediction and observation for the evolution of PSR 1913+16's orbit (Weisberg & Taylor 2005). Additional inspiraling systems have been discovered; in all cases for which we have enough data to discern period evolution, the data agree with theory to within measurement precision (Stairs et al. 1998; Nice et al. 2005; Jacoby et al. 2006; Kramer & Stairs 2008; Bhat, Bailes & Verbiest 2008). At least one additional recently discovered system is likely to show a measurable inspiral in the next few years (Kasian 2008). These measurements have validated our theory of GW generation and are among our most powerful tests of GR.

Measuring GWs with the new generations of detectors requires even more complete models for their waveforms and, hence, complete models of a binary's evolution. Motivated by this, our theoretical understanding of merging compact binaries and their GWs has grown tremendously. The purpose of this review is to summarize what we have learned about these systems and their waves, focusing on theory but connecting it to current and planned observations. We review the analytic and numerical toolkits that have been developed to model these binaries, discuss the different regimes in which these tools can be used, and summarize what has been learned about their evolution and waves. We begin by first examining compact binaries as astrophysical objects, turning next to how they are treated within the theory of GR.

1.2. Compact Binaries: The Astrophysical View

From the standpoint of GR, all compact binary systems are largely the same until their members come into contact, modulo the value of parameters such as the members' masses and spins and the orbital period at a given moment. This means that we only need one theoretical framework to model any compact binary that we encounter in nature. From the standpoint of astrophysics, though, all compact binary systems are not the same: A $1.4\,M_\odot - 1.4\,M_\odot$ neutron star binary forms in very different processes than those that form a $10^6\,M_\odot - 10^6\,M_\odot$ black hole binary. In this section, we summarize the astrophysical wisdom regarding the various compact binary systems that should be strong generators of GWs.

Compact binaries are organized most naturally by their masses. At the low end we have stellar-mass binaries, which include the binary pulsars discussed in the previous section. The data on binaries on this end are quite solid, thanks to the ability to link models for the birth and evolution of these systems to observations. At least some fraction of short gamma-ray bursts are likely to be associated with the mergers of neutron star–neutron star (NS-NS) or black hole–neutron star (BH-NS) systems (Eichler et al. 1989; Fox et al. 2005). Gamma-ray telescopes may already be telling us about compact binary mergers many times per year (Nakar, Gal-Yam & Fox 2006).

There is also evidence that nature produces supermassive binaries, in which the members are black holes with $M \sim 10^6 - 10^9 \, M_\odot$ such as are found at the centers of galaxies. As described in more detail below, theoretical arguments combining hierarchical galaxy growth scenarios with the hypothesis that most galaxies host black holes generically predict the formation of such binaries. We have now identified quite a few systems with properties indicating that they may host such binaries. The evidence includes active galaxies with double cores (Komossa et al. 2003, Maness et al. 2004, Rodriguez et al. 2006); systems with doubly peaked emission lines (Zhou et al. 2004, Gerke et al. 2007); helical radio jets, interpreted as the precession or modulation of a jet due to binarity (Begelman, Blandford & Rees 1980; Conway & Wrobel 1995; Lobanov & Roland 2005); and systems that appear to be periodic or semiperiodic, such as the blazar OJ287 (Valtonen et al. 2008). There are also sources that suggest the system hosted a binary that recently merged, leading to the spin flip of a radio jet (Merritt & Ekers 2002) or to the interruption and later restarting of accretion activity (Liu, Wu & Cao 2003). As surveys go deeper and resolution improves, we may expect the catalog of candidate supermassive black hole binaries to expand.

Turn now from the observational evidence to theoretical models. If we assume that our Galaxy is typical, and that the inferred density of NS-NS systems in the Milky Way should carry over to similar galaxies (correcting for factors such as typical stellar age and the proportion of stars that form neutron stars), then we can estimate the rate at which binary systems merge in the universe. Narayan, Piran & Shemi (1991) and Phinney (1991) first performed such estimates, finding a middle-of-the-road estimate that about three binaries per year merge to a distance of 200 Mpc. More recent calculations based on later surveys and observations of NS-NS systems have amended this number somewhat; the total number expected to be measured by advanced detectors is in the range of several tens per year [see, e.g., Kalogera et al. (2007) for a detailed discussion of methodology and Kim, Kalogera & Lorimer (2006) for a summary].

Population synthesis gives us a second way to model the distribution of stellar mass compact binaries. Such calculations combine data on the observed distribution of stellar binaries with models for how stars evolve. Begin with a pair of main sequence stars. The more massive star evolves into a giant, transfers mass onto its companion, and then goes supernova, leaving a neutron star or black hole. After some time, the companion also evolves into a giant and transfers mass onto its compact companion (and may be observable as a high-mass X-ray binary). In almost all cases, the compact companion is swallowed by the envelope of the giant star, continuing to orbit the giant's core. The orbiting compact body can then unbind the envelope, leaving the giant's core behind to undergo a supernova explosion and form a compact remnant. See Tauris & van den Heuvel (2006), especially their figure 16.12, for further discussion.

An advantage of population synthesis is that one can estimate the rate of formation and merger for systems that we cannot at present observe, such as stellar mass black hole–black hole (BH-BH) binaries, or for which we have only circumstantial evidence, such as neutron star–black hole (NS-BH) binaries (which presumably form some fraction of short gamma-ray bursts). A disadvantage is that the models of stellar evolution in binaries have many uncertainties. There are multiple branch points in the scenario described, such as whether the binary remains bound

following each supernova and whether the binary survives common envelope evolution. As a consequence, the predictions of calculations based on population synthesis can be quite diverse. Though different groups generally agree well with the rates for NS-NS systems (by design), their predictions for NS-BH and BH-BH systems differ by quite a bit (Yungelson & Portegies Zwart 1998, Postnov & Prokhorov 1999). New data are needed to clear the theoretical cobwebs.

Binaries can also form dynamically through many-body interactions in dense environments, such as globular clusters. In such a cluster, the most massive bodies tend to sink through mass segregation (Spitzer 1969); as such, the core of the cluster becomes populated with the heaviest bodies, either stars that will evolve into compact objects or the compact objects themselves. As those objects interact with one another, they tend to form massive binaries; calculations show that the production of BH-BH binaries is particularly favored. It is thus likely that globular clusters act as "engines" for the production of massive compact binaries (Portegies Zwart & McMillan 2000; O'Leary, O'Shaughnessy & Rasio 2007; Mackey et al. 2008).

As mentioned above, the hierarchical growth scenario for galaxies, coupled with the hypothesis that most galactic bulges host large black holes (Kormendy & Gebhardt 2001, Ferrarese 2002), generically predicts the formation of supermassive binaries, especially at high redshifts when mergers were common. The first careful discussion of this scenario was by Begelman, Blandford & Rees (1980). In order for the black holes to get close enough to merge with one another due to GW emission, the black holes hosted by the merging galaxies must sink, via dynamical friction, into the center of the newly merged object. The binary system thus formed is typically very widely separated and only hardens through interactions with field stars (ejecting them from the center). For some time, it was unclear whether there would be enough stars to bring the holes close enough that they would be strong GW emitters. It is now thought that, at least on the low end of the black hole mass function ($M \lesssim 10^6 - 10^7 \, M_\odot$), this so-called last parsec problem is not such a problem. Quite a few mechanisms have been found to carry the binary into the regime where GWs can merge the binary (Armitage & Natarajan 2002, Merritt & Milosavljević 2005). It is now fairly common to assume that some mechanism will bring a binary's members into the regime where they can merge. Much theoretical activity in recent years has thus focused on the coevolution of black holes and galaxies in hierarchical scenarios (Menou, Haiman & Narayanan 2001; Yu & Tremaine 2002; Volonteri, Haardt & Madau 2003). Galaxy mergers appear to be a natural mechanism to bring "fuel" to one or both black holes, igniting quasar activity; the formation of a binary may thus be associated with the duty cycle of quasars (Haiman, Ciotti & Ostriker 2004; Hopkins et al. 2008; Di Matteo et al. 2008). Such scenarios typically find that most black hole mergers come at fairly high redshift ($z \gtrsim 3$ or so) and that the bulk of a given black hole's mass is due to gas it has accreted over its growth.

A subset of binaries in the supermassive range are of particular interest to the relativity theorist. These binaries form by the capture of a "small" ($1 - 100 \, M_\odot$) compact object onto an orbit around the black hole in a galactic center. Such binaries form dynamically through stellar interactions in the core (Sigurdsson & Rees 1997, Hopman & Alexander 2005); the formation rate predicted by most models is typically $\sim 10^{-7}$ extreme mass ratio binaries per galaxy per year (Hopman & Alexander 2005). If the inspiraling object is a white dwarf or star, it could tidally disrupt as it comes close to the massive black hole, producing an X-ray or gamma-ray flare (Rathore, Blandford & Broderick 2005; Menou, Haiman & Kocsis 2008; Rosswog, Ramirez-Ruiz & Hix 2008). If the inspiraling object is a neutron star or black hole, it will be swallowed whole by the large black hole. As such, it will almost certainly be electromagnetically quiet; however, as is discussed in more detail below and in Section 4, its GW signature will be loud, making it a particularly interesting target for GW observers.

1.3. Compact Binaries: The Relativity View

Despite the diverse astrophysical paths to forming a compact binary, the end result always looks more or less the same from the standpoint of gravity. We now briefly outline the general features of binary evolution in GR. As described near the beginning of Section 1, in GR a binary is not so much described by two bodies as by one spacetime. The methods used to describe this spacetime depend on the extent to which the two-body description is useful.

Although it is something of an oversimplification, it is useful to divide the evolution of a binary into two or three broad epochs, following Flanagan & Hughes (1998). First is the binary's inspiral, in which its members are widely separated and can be readily defined as a pair of distinct bodies. During the inspiral, the binary's mean separation gradually decreases owing to the secular evolution of its orbital energy and angular momentum by the backreaction of gravitational radiation. The bodies eventually come together, merging into a single highly dynamical and asymmetric object. We call the merger the final transition from two bodies into one. If the final state of the system is a black hole, then its last dynamics are given by a ringdown as that black hole settles down from the highly distorted postmerger state into a Kerr black hole as required by the "no-hair" theorems of GR (Carter 1971, Robinson 1975).

How we solve the equations of GR to model a binary and its GWs depends upon the epoch that describes it. When the binary is widely separated, the post-Newtonian (pN) expansion of GR works very well. In this case, the Newtonian potential $\phi \equiv GM/rc^2$ (where $M = m_1 + m_2$ is the total mass of a binary, and r is the orbital separation) can be taken to be a small parameter. Indeed, we must always have $r \gtrsim$ (a few) $\times GM/c^2$: The closest the members of the binary can come is set by their physical size, which has a lower bound given by the radius they would have if they were black holes. The pN expansion is what we get by iterating GR's field equations from the Newtonian limit to higher order in ϕ. We review the basic principles of the pN expansion and summarize important results in Section 5.

Some binaries, such as the extreme mass ratio captures described in Section 1.2, will have $m_1 \ll m_2$. For these cases, the reduced mass ratio $\eta \equiv \mu/M = m_1 m_2/(m_1 + m_2)^2$ can define a perturbative expansion. In this limit, one can treat the binary's spacetime as an exact background solution with mass M (e.g., that of a black hole) perturbed by a smaller mass μ. By expanding GR's field equations around the exact background, one can typically derive tractable equations describing the perturbation and its evolution; those perturbations encode the dynamical evolution of the binary and its evolution. We discuss perturbative approaches to binary modeling in Section 4.

For some binaries, no approximation scheme is useful. Consider, for example, the last moments of two black holes coming together and fusing into a single body. In these moments, the spacetime can be highly dynamical and asymmetric; no obvious small parameter organizes our thinking about the spacetime. Instead, one must simply solve Einstein's field equations as exactly as possible using numerical methods. The essential question this field of numerical relativity asks is how one can take a "slice" of spacetime (that is, a single 3D moment of time) and use the field equations to understand how that spacetime evolves into the future. This requires us to explicitly split "spacetime" into "space" and "time." Progress in numerical relativity has exploded in recent years. Since 2005, practitioners have moved from being able to just barely model a single binary orbit for a highly symmetric system to modeling multiple orbits and the final coalescence for nearly arbitrary binary masses and spins. We summarize the major principles of this field and review the explosion of recent activity in Section 6.

Roughly speaking, for comparable mass binaries, pN methods describe the inspiral, and numerical relativity describes the merger. The line dividing these regimes is fuzzy. A technique called

the effective one-body (EOB) approximation blurs it even further by making it possible to extend pN techniques beyond their naïve range of validity (Damour 2008), at least when both members of the binary are black holes. [When at least one of the members is a neutron star, at some point the nature of the neutron star fluid will have an impact. Detailed numerical modeling will then surely be critical; see Shibata & Uryū (2006) and Etienne et al. (2008) for examples of recent progress.] Detailed tests show that using EOB methods greatly extends the domain for which analytical waveform models can accurately model numerical relativity waveforms (Buonanno et al. 2007, Damour et al. 2008). A brief discussion of these techniques is included in Sections 5 and 6.

Finally, it is worth noting that the ringdown waves that come from the last dynamics of a newly born black hole can also be modeled using perturbation theory. The spacetime is accurately modeled as a black hole plus a small deviation. Perturbation theory teaches us that black holes ring in a series of modes, with frequencies and damping times that are controlled by the mass and the spin of the black hole (Leaver 1985). Any deviation from an exact black hole solution is carried away by such modes, enforcing the black hole no-hair theorems (Price 1972a,b). We do not say much about the ringdown in this review, except to note that the last waves that come from numerical relativity simulations have been shown to agree excellently with these perturbative calculations.

1.4. Notation and Conventions

The underlying theory of GWs is general relativity; we review the crucial concepts for this review in Section 2. Because multiple conventions are often used in the GR literature, we first describe our notation and conventions.

Throughout this review, Greek indices denote spacetime components of tensors and vectors. These indices run over (0, 1, 2, 3), with 0 generally denoting time t and (1, 2, 3) denoting spatial directions. Spacetime vectors are sometimes written with an overarrow:

$$\vec{A} = \{A^{\mu}\} \doteq (A^0, A^1, A^2, A^3). \tag{1}$$

Equation 1 should be read as "The vector $\vec{A}$ has components A^{μ} whose values in a specified coordinate system are A^0, A^1, A^2, and A^3." Lowercase Latin indices denote spatial components. Spatial vectors are written in boldface:

$$\mathbf{a} = \{a^i\} \doteq (a^1, a^2, a^3). \tag{2}$$

We use the Einstein summation convention throughout, meaning that repeated adjacent indices in superscript and subscript positions are to be summed:

$$A^{\mu} B_{\mu} \equiv \sum_{\mu=0}^{3} A^{\mu} B_{\mu}. \tag{3}$$

Indices are raised and lowered using the metric of spacetime (discussed in more detail in Section 2) as a raising or lowering operator:

$$A^{\mu} B_{\mu} = g_{\mu\nu} A^{\mu} B^{\nu} = A_{\nu} B^{\nu} = g^{\mu\nu} A_{\mu} B_{\nu}. \tag{4}$$

When we discuss the linearized limit of GR (particularly in Section 3), it is useful to work in coordinates such that the spacetime metric can be written as that of special relativity plus a small perturbation:

$$g_{\mu\nu} = \eta_{\mu\nu} + h_{\mu\nu}, \tag{5}$$

where $\eta_{\mu\nu} = \text{diag}(-1,1,1,1)$. This means that the spatial part of the background metric is the Kronecker delta δ_{ij}. For certain calculations in linearized theory, it is useful to abuse the Einstein summation convention and sum over repeated adjacent spatial indices regardless of position:

$$\sum_{i=1}^{3} a_i b^i = a_i b^i = a_i b_i = a^i b^i. \tag{6}$$

This is allowable because using the Kronecker delta for the spatial part of the metric means $a^i = a_i$ to this order.

Throughout this review, we abbreviate the partial derivative

$$\frac{\partial}{\partial x^\mu} \equiv \partial_\mu. \tag{7}$$

With this notation defined, we can write $\partial^\mu = g^{\mu\nu} \partial_\nu$.

Finally, it is common in GR research to use units in which the gravitational constant G and the speed of light c are set to 1. This has the advantage that mass, space, and time have the same units, but can be confusing when applied to astrophysical systems. In deference to the astronomical audience of this review, we have put Gs and cs back into the relativity formulas. An exception to the rule that $G = c = 1$ everywhere is Shapiro & Teukolsky (1983), especially their chapter 15.

2. SYNOPSIS OF GENERAL RELATIVITY

General relativity describes gravity as geometry. The foundation of this is the metric, which provides a notion of spacetime distance. Suppose event A occurs at coordinate x^α, and event B at $x^\alpha + dx^\alpha$. The proper spacetime separation, ds, between A and B is given by

$$ds^2 = g_{\alpha\beta} dx^\alpha dx^\beta. \tag{8}$$

The metric $g_{\alpha\beta}$ translates the information in coordinates, which can be arbitrary, into a proper quantity, which can be measured. In the limit of special relativity, $g_{\alpha\beta}$ becomes $\eta_{\alpha\beta}$ (defined in Section 1.4). The general spacetime metric is determined by the distribution of mass and energy; we describe how to compute it below. It will sometimes be useful to work with the inverse metric $g^{\alpha\beta}$, defined by

$$g^{\alpha\beta} g_{\beta\gamma} = \delta^\alpha_\gamma. \tag{9}$$

The metric also takes inner products between vectors and tensors:

$$\vec{A} \cdot \vec{B} = g_{\alpha\beta} A^\alpha B^\beta. \tag{10}$$

$\vec{A}$ is timelike if $\vec{A} \cdot \vec{A} < 0$, spacelike if $\vec{A} \cdot \vec{A} > 0$, and lightlike or null if $\vec{A} \cdot \vec{A} = 0$.

Consider a worldline or spacetime trajectory $z^\mu(\tau)$, where τ is proper time (time as measured by an observer on that worldline). The vector $u^\mu \equiv dz^\mu/d\tau$ is the tangent to the worldline. If u^μ is timelike, it is the 4-velocity of an observer following the worldline, and is normalized $u^\mu u_\mu = -1$. Suppose the worldline extends from A to B. The total spacetime separation between these points is

$$s = \int_A^B d\tau \sqrt{g_{\alpha\beta} u^\alpha u^\beta}. \tag{11}$$

We now extremize s: We fix the endpoints, allow quantities under the integral to vary, but require the variation to be stationary (so that $\delta s = 0$). The u^α that extremizes s is given by the geodesic equation:

$$\frac{du^\alpha}{d\tau} + \Gamma^\alpha_{\beta\gamma} u^\beta u^\gamma = 0. \tag{12}$$

We have introduced the connection $\Gamma^{\alpha}_{\beta\gamma}$; it is built from the metric by

$$\Gamma^{\alpha}_{\beta\gamma} = \frac{1}{2} g^{\alpha\mu} \left(\partial_\gamma g_{\mu\beta} + \partial_\beta g_{\gamma\mu} - \partial_\mu g_{\beta\gamma} \right). \tag{13}$$

Geodesics are important for our discussion because freely falling bodies follow geodesics of space-time in general relativity. Geodesics express the rule that "spacetime tells bodies how to move."

Timelike geodesics describe material bodies. Null geodesics, for which $u^\mu u_\mu = 0$, describe massless bodies or light rays. Our discussion above describes null geodesics, with one modification: We cannot parameterize a null worldline with τ because proper time is not meaningful for a speed of light trajectory. Instead, one uses an affine parameter λ that uniformly ticks along that trajectory. A convenient choice is to set $u^\alpha \equiv dx^\alpha/d\lambda$ to be the 4-momentum of our radiation or massless body. With this choice, our discussion describes null trajectories just as well as timelike ones.

The connection also defines the covariant derivative of a vector or tensor:

$$\begin{aligned}
\nabla_\alpha A^\beta &= \partial_\alpha A^\beta + A^\mu \Gamma^{\beta}_{\alpha\mu}, \\
\nabla_\alpha A_\beta &= \partial_\alpha A_\beta - A_\mu \Gamma^{\mu}_{\alpha\beta}, \\
\nabla_\alpha A^\beta_\gamma &= \partial_\alpha A^\beta_\gamma + A^\mu_\gamma \Gamma^{\beta}_{\alpha\mu} - A^\beta_\mu \Gamma^{\mu}_{\alpha\gamma}.
\end{aligned} \tag{14}$$

The pattern continues as we add indices. This derivative follows by comparing vectors and tensors that are slightly separated by parallel transporting them together to make the comparison; the connection encodes the twists of our curved geometry. Using the covariant derivative, the geodesic equation can be written

$$u^\beta \nabla_\beta u^\alpha = 0. \tag{15}$$

In curved spacetime, nearby geodesics diverge. Because a geodesic describes a freely falling body, the rate at which geodesics diverge describes tides. Let ξ^α be the displacement between geodesics. Then the rate of divergence is given by

$$\frac{D^2 \xi^\alpha}{d\tau^2} = R^{\alpha}_{\beta\gamma\delta} u^\beta u^\gamma \xi^\delta. \tag{16}$$

We have introduced the Riemann curvature tensor,

$$R^{\alpha}_{\beta\gamma\delta} = \partial_\gamma \Gamma^{\alpha}_{\beta\delta} - \partial_\delta \Gamma^{\alpha}_{\beta\gamma} + \Gamma^{\alpha}_{\mu\gamma} \Gamma^{\mu}_{\beta\delta} - \Gamma^{\alpha}_{\mu\delta} \Gamma^{\mu}_{\beta\gamma}. \tag{17}$$

Some variants of Riemann are important. First, there is the Ricci curvature,

$$R_{\alpha\beta} = R^{\mu}_{\alpha\mu\beta}. \tag{18}$$

Ricci is the trace of Riemann. Taking a further trace gives us the Ricci scalar,

$$R = R^{\mu}_{\mu}. \tag{19}$$

The Ricci tensor and Ricci scalar combine to produce the Einstein curvature,

$$G_{\alpha\beta} = R_{\alpha\beta} - \frac{1}{2} g_{\alpha\beta} R. \tag{20}$$

The Riemann curvature satisfies the Bianchi identity,

$$\nabla_\gamma R_{\alpha\beta\mu\nu} + \nabla_\beta R_{\gamma\alpha\mu\nu} + \nabla_\alpha R_{\beta\gamma\mu\nu} = 0. \tag{21}$$

By tracing over certain combinations of indices, the Bianchi identity implies

$$\nabla^\alpha G_{\alpha\beta} = 0, \tag{22}$$

a result sometimes called the contracted Bianchi identity.

So far, we have mostly described the mathematics of curved geometry. We must also introduce tools to describe matter and fields. The most important tool is the stress-energy tensor,

$$T^{\mu\nu} \equiv \text{flux of momentum } p^{\mu} \text{ in the } x^{\nu} \text{ direction.} \tag{23}$$

An observer who uses coordinates (t, x^i) to make local measurements interprets the components of this tensor as

$$T^{tt} \equiv \text{Local energy density,} \tag{24}$$

$$T^{ti} \equiv \text{Local energy flux (times } c), \tag{25}$$

$$T^{it} \equiv \text{Local momentum density (times } c), \tag{26}$$

$$T^{ij} \equiv \text{Local momentum flux (times } c^2); \quad T^{ii} \text{ acts as pressure.} \tag{27}$$

(The factors of c in Equations 25–27 ensure that the components of $T^{\mu\nu}$ have the same dimension.) Local conservation of energy and momentum is expressed by

$$\nabla_{\mu} T^{\mu\nu} = 0. \tag{28}$$

In GR, we generally lose the notion of global energy conservation: We cannot integrate Equation 28 over an extended region to add up the total energy and momentum. This is because $\nabla_{\mu} T^{\mu\nu}$ is a spacetime vector, and in curved spacetime one cannot unambiguously compare widely separated vectors.

Einstein's hypothesis is that stress energy is the source of spacetime curvature. If $T^{\mu\nu}$ is our source, then the curvature must likewise be divergence free. The contracted Bianchi identity (22) shows us that the Einstein tensor is the curvature we need. This logic yields the Einstein field equation,

$$G_{\mu\nu} = \frac{8\pi G}{c^4} T_{\mu\nu}. \tag{29}$$

The factor $8\pi G/c^4$ guarantees that this equation reproduces Newtonian gravity in an appropriate limit. Note its value,

$$\frac{G}{c^4} = 8.26 \times 10^{-50} \frac{\text{cm}^{-2}}{\text{erg/cm}^3}. \tag{30}$$

It takes an enormous amount of energy density to produce spacetime curvature (measured in inverse length squared). Note that the reciprocal of this quantity, times c, has the dimensions of power $\frac{c^5}{G} = 3.63 \times 10^{59} \text{ erg sec}^{-1}$. This is the scale for the power that is generated by a GW source.

3. GRAVITATIONAL-WAVE BASICS

We now give a brief description of how gravitational waves arise in GR. Our purpose is to introduce the main ideas of this field and also provide some results against which the more complete calculations we discuss later can be compared.

3.1. Leading Waveform

Begin with weak gravity, so that spacetime is nearly that of special relativity,

$$g_{\alpha\beta} = \eta_{\alpha\beta} + b_{\alpha\beta}. \tag{31}$$

Take the correction to flat spacetime to be small so that we can linearize about $\eta_{\alpha\beta}$. Consider, for example, raising and lowering indices:

$$b^{\alpha\beta} \equiv g^{\alpha\mu} g^{\beta\nu} b_{\mu\nu} = \eta^{\alpha\mu} \eta^{\beta\nu} b_{\mu\nu} + \mathcal{O}(b^2). \tag{32}$$

Because we only keep quantities to first order in b, we consistently use the flat metric to raise and lower indices for quantities related to the geometry.

Applying this logic repeatedly, we build the linearized Einstein tensor,

$$G_{\alpha\beta} = \frac{1}{2} \left(\partial_\alpha \partial^\mu b_{\mu\beta} + \partial_\beta \partial^\mu b_{\mu\alpha} - \partial_\alpha \partial_\beta b - \Box b_{\alpha\beta} + \eta_{\alpha\beta} \Box b - \eta_{\alpha\beta} \partial^\mu \partial^\nu b_{\mu\nu} \right), \tag{33}$$

where $b \equiv \eta^{\alpha\beta} b_{\alpha\beta}$ is the trace of $b_{\alpha\beta}$, and $\Box \equiv \eta^{\alpha\beta} \partial_\alpha \partial_\beta$ is the flat spacetime wave operator.

Equation 33 is rather messy. We clean it up in two steps. The first is pure sleight of hand: We introduce the trace-reversed metric perturbation

$$\bar{b}_{\alpha\beta} \equiv b_{\alpha\beta} - \frac{1}{2} \eta_{\alpha\beta} b. \tag{34}$$

With this definition, Equation 38 becomes

$$G_{\alpha\beta} = \frac{1}{2} \left(\partial_\alpha \partial^\mu \bar{b}_{\mu\beta} + \partial_\beta \partial^\mu \bar{b}_{\mu\alpha} - \Box \bar{b}_{\alpha\beta} - \eta_{\alpha\beta} \partial^\mu \partial^\nu b_{\mu\nu} \right). \tag{35}$$

Next, we take advantage of the gauge-freedom of linearized gravity. Recall that in electrodynamics, if one adjusts the potential by the gradient of a scalar, $A_\mu \to A_\mu - \partial_\mu \Lambda$, then the field tensor $F_{\mu\nu} = \partial_\mu A_\nu - \partial_\nu A_\mu$ is unchanged. In linearized GR, a similar operation follows by adjusting one's coordinates: If one changes coordinates $x^\alpha \to x^\alpha + \xi^\alpha$ (requiring $\partial_\mu \xi^\alpha \ll 1$), then

$$b_{\mu\nu} \to b_{\mu\nu} - \partial_\mu \xi_\nu - \partial_\nu \xi_\mu. \tag{36}$$

One can easily show (see, e.g., Carroll 2004, section 7.1) that changing gauge leaves the Riemann tensor (and thus all tensors derived from it) unchanged.

We take advantage of our gauge freedom to choose ξ^α so that

$$\partial^\mu \bar{b}_{\mu\nu} = 0. \tag{37}$$

This is called the Lorenz gauge in analogy with the electrodynamic Lorenz gauge condition $\partial^\mu A_\mu = 0$. This simplifies our Einstein tensor considerably, yielding

$$G_{\alpha\beta} = -\frac{1}{2} \Box \bar{b}_{\alpha\beta}. \tag{38}$$

The Einstein equation for linearized gravity thus takes the simple form

$$\Box \bar{b}_{\alpha\beta} = -\frac{16\pi G}{c^4} T_{\alpha\beta}. \tag{39}$$

Any linear equation of this form can be solved using a radiative Green's function (e.g., Jackson 1975, section 12.11). Doing so yields

$$\bar{b}_{\alpha\beta}(\mathbf{x}, t) = \frac{4G}{c^4} \int \frac{T_{\alpha\beta}(\mathbf{x}', t - |\mathbf{x} - \mathbf{x}'|/c)}{|\mathbf{x} - \mathbf{x}'|} d^3 x'. \tag{40}$$

In this equation, $\mathbf{x}$ is the field point, where $\bar{b}_{\alpha\beta}$ is evaluated, and $\mathbf{x}'$ is a source point, the coordinate we integrate over the source's spatial extent. Notice that the solution at t depends on what happens to the source at retarded time $t - |\mathbf{x} - \mathbf{x}'|/c$. Information must causally propagate from $\mathbf{x}'$ to $\mathbf{x}$.

Equation 40 is formally an exact solution to the linearized Einstein field equation. However, it has a serious problem: It gives the impression that every component of the metric perturbation is

radiative. This is an unfortunate consequence of our gauge. Just as one can choose a gauge such that an isolated point charge has an oscillatory potential, the Lorenz gauge we have used makes all components of the metric appear radiative, even if they are static. [In the electromagnetic case, it is unambiguous which field components are radiative and which are static. Similarly, one can always tell which Riemann curvature components are radiative and which are static. Eddington (1922) appears to have been the first to use the curvature tensor to categorize the gravitational degrees of freedom in this way.]

Fortunately, it is not difficult to see that only a subset of the metric represents the truly radiative degrees of freedom in all gauges. We only quote the result here; interested readers can find the full calculation done by Flanagan & Hughes (2005, Section 2.2): Given a solution $h_{\alpha\beta}$ to the linearized Einstein field equations, only the spatial, transverse, and traceless components h_{ij}^{TT} describe the spacetime's gravitational radiation in a gauge-invariant manner. (The other components can be regarded as longitudinal degrees of freedom, much like the Coulomb potential of electrodynamics.) Traceless means

$$\delta_{ij} h_{ij}^{\mathrm{TT}} = 0; \tag{41}$$

transverse means

$$\partial_i h_{ij}^{\mathrm{TT}} = 0. \tag{42}$$

This condition tells us that h_{ij}^{TT} is orthogonal to the direction of the wave's propagation. Expanding h_{ij}^{TT} in Fourier modes shows that Equation 42 requires h_{ij}^{TT} to be orthogonal (in space) to each mode's wave vector $\mathbf{k}$.

Conditions (i.e., Equations 41 and 42) make it simple to construct h_{ij}^{TT} given some solution h_{ij} to the linearized field equations. Let n_i denote components of the unit vector along the wave's direction of propagation. The tensor

$$P_{ij} = \delta_{ij} - n_i n_j \tag{43}$$

projects spatial components orthogonal to $\mathbf{n}$. It is then simple to verify that

$$h_{ij}^{\mathrm{TT}} = h_{kl} \left(P_{ki} P_{lj} - \frac{1}{2} P_{kl} P_{ij} \right) \tag{44}$$

represents the transverse and traceless metric perturbation.

The simplest example solution to Equation 44 can be built by going back to Equation 40 and focusing on the spatial components:

$$\bar{h}_{ij} = \frac{4G}{c^4} \int \frac{T_{ij}(\mathbf{x}', t - |\mathbf{x} - \mathbf{x}'|/c)}{|\mathbf{x} - \mathbf{x}'|} d^3 x'. \tag{45}$$

Consider a very distant source, putting $|\mathbf{x} - \mathbf{x}'| \simeq R$:

$$\bar{h}_{ij} \simeq \frac{4}{R} \frac{G}{c^4} \int T_{ij}(\mathbf{x}', t - R/c) d^3 x'. \tag{46}$$

To proceed, we invoke an identity. Using the fact that $\nabla^\mu T_{\mu\nu} = 0$ goes to $\partial^\mu T_{\mu\nu} = 0$ in linearized theory and in our chosen coordinates, we have

$$\partial^t T_{tt} + \partial^j T_{jt} = 0, \quad \partial^t T_{tj} + \partial^i T_{ij} = 0. \tag{47}$$

Combine these identities with the fact that $\partial^t = -\partial_t$; use integration by parts to convert volume integrals to surface integrals; discard those integrals by taking the surface outside our sources. We then find

$$\int T_{ij}(\mathbf{x}', t) d^3 x' = \frac{1}{2} \frac{d^2}{dt^2} \int x^{i'} x^{j'} T_{tt}(\mathbf{x}', t) d^3 x' \equiv \frac{1}{2} \frac{d^2}{dt^2} I_{ij}(t). \tag{48}$$

We have introduced here the quadrupole moment I_{ij}. This allows us to at last write the transverse-traceless waveform as

$$b_{ij}^{\mathrm{TT}} = \frac{2}{R}\frac{G}{c^4}\frac{d^2 I_{kl}}{dt^2}\left(P_{ik}P_{jl} - \frac{1}{2}P_{kl}P_{ij}\right). \qquad (49)$$

It is straightforward to show that the trace $I \equiv I_{ii}$ does not contribute to Equation 49, so it is common to use the reduced quadrupole moment,

$$\mathcal{I}_{ij} = I_{ij} - \frac{1}{3}\delta_{ij}I. \qquad (50)$$

The waveform then takes the form in which it is usually presented,

$$b_{ij}^{\mathrm{TT}} = \frac{2}{R}\frac{G}{c^4}\frac{d^2 \mathcal{I}_{kl}}{dt^2}\left(P_{ik}P_{jl} - \frac{1}{2}P_{kl}P_{ij}\right), \qquad (51)$$

that is, the quadrupole formula for GW emission.

A more accurate approximation than $|\mathbf{x} - \mathbf{x}'| \simeq R$ is

$$|\mathbf{x} - \mathbf{x}'| \simeq R - \mathbf{n}\cdot\mathbf{x}', \qquad (52)$$

where $\mathbf{n}$ is the unit vector pointing from $\mathbf{x}'$ to $\mathbf{x}$. Revisiting the calculation, we find that Equation 51 is the first term in a multipolar expansion for the radiation. Detailed formulae and notation can be found in Thorne (1980, section IVA). Schematically, the resulting waveform can be written

$$b^{\mathrm{TT}} = \frac{1}{R}\frac{G}{c^2}\sum_{l=2}^{\infty}\left\{\frac{\mathcal{A}_l}{c^l}\frac{d^l \mathcal{I}_l}{dt^l} + \frac{\mathcal{B}_l}{c^{l+1}}\frac{d^l \mathcal{S}_l}{dt^l}\right\}^{\mathrm{STF}}. \qquad (53)$$

We have hidden various factorials of l in the coefficients $\mathcal{A}_l$ and $\mathcal{B}_l$; the superscript "STF" means to symmetrize the result on any free indices and remove the trace.

The symbol $\mathcal{I}_l$ stands for the lth mass moment of the source. Thorne (1980) precisely defines $\mathcal{I}_l$; for our purposes, it is enough to note that it represents an integral of l powers of length over the source's mass density ρ:

$$\mathcal{I}_l \sim \int \rho(x')(x')^l\, d^3x'. \qquad (54)$$

The mass moment plays a role in gravitational radiation similar to that played by the electric charge moment in electrodynamics. The symbol $\mathcal{S}_l$ describes the lth mass-current moment; it represents an integral of l powers of length over the source's mass-current $\mathbf{J} = \rho\mathbf{v}$, where $\mathbf{v}$ describes a source's internal motions:

$$\mathcal{S}_l \sim \int \rho(x')v(x')(x')^l\, d^3x'. \qquad (55)$$

$\mathcal{S}_l$ plays a role similar to the magnetic moment.

The similarity of the multipolar expansion (Equation 53) for GWs to that for electromagnetic radiation should not be a surprise; after all, our linearized field equation (Equation 39) is very similar to Maxwell's equation for the potential A_μ (modulo an extra index and a factor of four). One should be cautious about taking this analogy too far. Though electromagnetic intuition applied to linearized theory works well to compute the GWs from a source, one must go beyond this linearized form to understand deeper aspects of this theory. In particular, one must go to higher order in perturbation theory to see how energy and angular momentum are carried from a radiating source. We now sketch how this works in GR.

3.2. Leading Energy Loss

Electromagnetic radiation carries a flux of energy and momentum described by the Poynting vector, $\mathbf{S} = (c/4\pi)\mathbf{E} \times \mathbf{B}$. Likewise, electromagnetic fields generate stresses proportional to $(|\mathbf{E}|^2 + |\mathbf{B}|^2)/8\pi$. The lesson to take from this is that the energy content of radiation should be quadratic in wave amplitude. Properly describing the energy content of radiation requires second-order perturbation theory. In this section, we discuss the key concepts and ideas in this analysis, which was first given by Isaacson (1968).

Begin by writing the spacetime,

$$g_{\alpha\beta} = \hat{g}_{\alpha\beta} + \epsilon h_{\alpha\beta} + \epsilon^2 j_{\alpha\beta}. \tag{56}$$

We have introduced a parameter ϵ whose formal value is 1; we use it to gather terms that are of the same order. Note that now we do not restrict the background to be flat. This introduces a conceptual difficulty: Measurements directly probe only the total spacetime $g_{\alpha\beta}$ (or a derived surrogate-like curvature), so how do we distinguish background $\hat{g}_{\alpha\beta}$ from perturbation? The answer is to use separation of length scales. Our background only varies on long length scales and timescales $\mathcal{L}, \mathcal{T}$; our perturbation varies on short length scales and timescales λ, τ. We require $\mathcal{L} \gg \lambda$ and $\mathcal{T} \gg \tau$. Let $\langle f \rangle$ denote a quantity f averaged over long scales; this averaging is well defined even for tensors up to errors $\mathcal{O}(\lambda^2/\mathcal{L}^2)$. Then, to first order in ϵ,

$$\hat{g}_{\alpha\beta} = \langle g_{\alpha\beta} \rangle, \tag{57}$$

$$h_{\alpha\beta} = g_{\alpha\beta} - \hat{g}_{\alpha\beta}. \tag{58}$$

The second-order contribution will be of order h^2, and (as we see below) will have contributions on both long and short scales.

Begin by expanding the Einstein tensor in ϵ. The result can be written

$$G_{\mu\nu}(g_{\alpha\beta}) = G^0_{\mu\nu}(\hat{g}_{\alpha\beta}) + \epsilon G^1_{\mu\nu}(h_{\alpha\beta}) + \epsilon^2 \left[G^2_{\mu\nu}(h_{\alpha\beta}) + G^1_{\mu\nu}(j_{\alpha\beta}) \right]. \tag{59}$$

For simplicity, take the spacetime to be vacuum—there are no nongravitational sources of stress and energy in the problem. We then require Einstein's equation, $G_{\mu\nu} = 0$, to hold at each order. The zeroth-order result,

$$G^0_{\mu\nu}(\hat{g}_{\alpha\beta}) = 0, \tag{60}$$

is just a statement that we assume our background to be a vacuum solution.

Expanding $G^1_{\mu\nu}(h_{\alpha\beta}) = 0$, we find

$$-\frac{1}{2}\hat{\Box}\bar{h}_{\alpha\beta} - \hat{R}_{\alpha\mu\beta\nu}\bar{h}^{\mu\nu} = 0, \tag{61}$$

where $\hat{\Box} \equiv \hat{g}^{\mu\nu}\hat{\nabla}_\mu\hat{\nabla}_\nu$ is the wave operator for $\hat{g}_{\mu\nu}$ (with $\hat{\nabla}_\mu$ the covariant derivative on $\hat{g}_{\mu\nu}$), $\hat{R}_{\alpha\mu\beta\nu}$ is the Riemann curvature built from $\hat{g}_{\mu\nu}$, and $\bar{h}_{\mu\nu} = h_{\mu\nu} - (1/2)\hat{g}_{\mu\nu}h$. Equation 61 is just the wave equation for radiation propagating on a curved background. The coupling between h and the background Riemann tensor describes a correction to the usual geometric optics limit.

Next, consider second order:

$$G^1_{\mu\nu}(j_{\alpha\beta}) = -G^2_{\mu\nu}(h_{\alpha\beta}). \tag{62}$$

To make sense of this, invoke separation of scales. The second-order perturbation has contributions on both scales:

$$j_{\alpha\beta} = \langle j_{\alpha\beta} \rangle + \delta j_{\alpha\beta}, \tag{63}$$

where $\langle j_{\alpha\beta}\rangle$ varies on long scales and $\delta j_{\alpha\beta}$ is oscillatory and varies on short scales. The second-order metric can now be written

$$g_{\alpha\beta} = g_{\alpha\beta}^{\mathcal{L}} + \epsilon b_{\alpha\beta} + \epsilon^2 \delta j_{\alpha\beta}, \tag{64}$$

where

$$g_{\alpha\beta}^{\mathcal{L}} \equiv \hat{g}_{\alpha\beta} + \epsilon^2 \langle j_{\alpha\beta}\rangle \tag{65}$$

is a corrected background, which includes all pieces that vary on long scales.

Now return to the Einstein equation (Equation 59), but consider its averaged value. Thanks to linearity, we can take the averaging inside the operator G^1:

$$\langle G_{\mu\nu}^1(b_{\alpha\beta})\rangle = G_{\mu\nu}^1(\langle b_{\alpha\beta}\rangle) = 0. \tag{66}$$

We have used here $\langle b_{\alpha\beta}\rangle = 0$. Putting all this together, we find

$$G_{\mu\nu}^0(\hat{g}_{\alpha\beta}) + \epsilon^2[\langle G_{\mu\nu}^2(b_{\alpha\beta})\rangle + G_{\mu\nu}^1(\langle j_{\alpha\beta}\rangle)] = 0. \tag{67}$$

Let us rewrite this as

$$G_{\mu\nu}(\hat{g}_{\alpha\beta} + \epsilon^2 \langle j_{\alpha\beta}\rangle) = -\epsilon^2 \langle G_{\mu\nu}^2(b_{\alpha\beta})\rangle, \tag{68}$$

or, putting $\epsilon = 1$,

$$G_{\mu\nu}(g_{\alpha\beta}^{\mathcal{L}}) = -\langle G_{\mu\nu}^2(b_{\alpha\beta})\rangle. \tag{69}$$

Equation 69 says that the second-order averaged Einstein tensor acts as a source for the long length-scale background spacetime. This motivates the definition

$$T_{\mu\nu}^{\mathrm{GW}} = -\frac{c^4}{8\pi G}\langle G_{\mu\nu}^2(b_{\alpha\beta})\rangle. \tag{70}$$

Choosing a gauge so that $\hat{\nabla}^\mu \bar{b}_{\mu\nu} = 0$, $T_{\mu\nu}^{\mathrm{GW}}$ takes a very simple form:

$$T_{\mu\nu}^{\mathrm{GW}} = \frac{c^4}{32\pi G}\langle \nabla_\mu b_{\alpha\beta} \nabla_\nu b^{\alpha\beta}\rangle. \tag{71}$$

This quantity is known as the Isaacson stress-energy tensor (Isaacson 1968).

3.3. The Newtonian, Quadrupole Waveform

A useful exercise is to consider a binary with Newtonian orbital dynamics that radiates GWs according to Equation 51. Further, allow the binary to slowly evolve by energy and angular momentum carried off in accordance with Equation 71.

Begin by considering such a binary with its members in circular orbit of separation R. This binary is characterized by orbital energy

$$E^{\mathrm{orb}} = \frac{1}{2}m_1 v_1^2 + \frac{1}{2}m_2 v_2^2 - \frac{Gm_1 m_2}{R} = -\frac{G\mu M}{2R}, \tag{72}$$

(where $M = m_1 + m_2$ and $\mu = m_1 m_2/M$) and orbital frequency

$$\Omega_{\mathrm{orb}} = \sqrt{\frac{GM}{R^3}}. \tag{73}$$

Next consider the energy that GWs carry from the binary to distant observers. When evaluated far from a source, Equation 71 gives a simple result for energy flux:

$$\frac{dE}{dA\,dt} = \frac{c^4}{32\pi G}\langle \partial_t b_{ij}^{\mathrm{TT}} \partial_k b_{ij}^{\mathrm{TT}}\rangle n^k. \tag{74}$$

Plugging in Equation 51 and integrating over the sphere, we find

$$\frac{dE}{dt}^{\text{GW}} = \int dA \frac{dE}{dA\,dt} = \frac{G}{5c^5} \left\langle \frac{d^3\mathcal{I}_{ij}}{dt^3} \frac{d^3\mathcal{I}_{ij}}{dt^3} \right\rangle. \tag{75}$$

For the Newtonian binary,

$$\mathcal{I}_{ij} = \mu \left(x_i x_j - \frac{1}{3} r^2 \delta_{ij} \right). \tag{76}$$

Inserting into Equation 75, we find

$$\frac{dE}{dt}^{\text{GW}} = \frac{32}{5} \frac{G}{c^5} \mu^2 R^4 \Omega^6. \tag{77}$$

We now assert that the binary evolves quasi-statically, meaning that any radiation carried off by GWs is accounted for by the evolution of its orbital energy:

$$\frac{dE}{dt}^{\text{orb}} + \frac{dE}{dt}^{\text{GW}} = 0. \tag{78}$$

We evaluate dE^{orb}/dt by allowing the orbital radius to slowly change in time,

$$\frac{dE}{dt}^{\text{orb}} = \frac{dE}{dR}^{\text{orb}} \frac{dR}{dt}. \tag{79}$$

Combining Equations 77–79, we find

$$R(t) = \left[\frac{256 G^3 \mu M^2 (t_c - t)}{5 c^5} \right]^{1/4}. \tag{80}$$

This, in turn, tells us that the orbital frequency changes according to

$$\Omega_{\text{orb}}(t) = \left[\frac{5 c^5}{256 (G\mathcal{M})^{5/3} (t_c - t)} \right]^{3/8}. \tag{81}$$

We have introduced the binary's chirp mass $\mathcal{M} \equiv \mu^{3/5} M^{2/5}$, so called because it sets the rate at which the binary sweeps upward in frequency or chirps. We have also introduced the coalescence time t_c, which formally describes when the separation goes to zero (equivalently, when the frequency goes to infinity).

Given the substantial eccentricity of many binaries, restriction to circular orbits may not seem particularly realistic. Including eccentricity means that our binary will have two evolving parameters (semimajor axis a and eccentricity e) rather than just one (orbital radius R). To track their evolution, we must separately compute the radiated energy and angular momentum (Peters & Mathews 1963, Peters 1964):

$$\frac{dE}{dt}^{\text{GW}} = \frac{G}{5c^5} \left\langle \frac{d^3\mathcal{I}_{ij}}{dt^3} \frac{d^3\mathcal{I}_{ij}}{dt^3} \right\rangle = \frac{32}{5} \frac{G}{c^5} \mu^2 a^4 \Omega^6 f(e), \tag{82}$$

$$\frac{dL_z^{\text{GW}}}{dt} = \frac{2G}{5c^5} \epsilon_{zjk} \left\langle \frac{d^2\mathcal{I}_{jm}}{dt^2} \frac{d^3\mathcal{I}_{km}}{dt^3} \right\rangle = \frac{32}{5} \frac{G}{c^5} \mu^2 a^4 \Omega^5 g(e). \tag{83}$$

Because the binary is in the x-y plane, the angular momentum is purely along the z axis. The eccentricity corrections $f(e)$ and $g(e)$ are given by

$$f(e) = \frac{1 + \frac{73}{24} e^2 + \frac{37}{96} e^4}{(1 - e^2)^{7/2}}, \quad g(e) = \frac{1 + \frac{7}{8} e^2}{(1 - e^2)^2}. \tag{84}$$

Using standard definitions relating the semimajor axis and eccentricity to the E and L_z, Equations 82 and 83 imply (Peters 1964)

$$\frac{da}{dt} = -\frac{64}{5} \frac{G^3}{c^5} \frac{\mu M^2}{a^3} f(e), \tag{85}$$

$$\frac{de}{dt} = -\frac{304}{15} e \frac{G^3}{c^5} \frac{\mu M^2}{a^4} \frac{1 + \frac{121}{304} e^2}{(1 - e^2)^{5/2}}. \tag{86}$$

It is then simple to compute the rate at which an eccentric binary's orbital period changes due to GW emission. This result is compared with data from investigations of GW generating binary pulsars.

Notice that a binary's eccentricity decreases: GWs tend to circularize orbits. Many binaries are expected to be essentially circular by the time their waves enter the sensitive band of many GW detectors; the restriction to circularity is thus quite useful. Exceptions are binaries that form, through capture processes, very close to merging. The extreme mass ratio inspirals discussed in Section 4 are a particularly interesting example of this.

We conclude this section by writing the gravitational waveform predicted for quadrupole emission from the Newtonian, circular binary. Evaluating Equation 51, we find that h_{ij} has two polarizations. These are traditionally labeled plus and cross from the lines of force associated with their tidal stretch and squeeze. Taking our binary to be a distance D from Earth, its waveform is written

$$h_+ = -\frac{2G\mathcal{M}}{c^2 D} \left(\frac{\pi G \mathcal{M} f}{c^3}\right)^{2/3} (1 + \cos^2 \iota) \cos 2\Phi_N(t),$$

$$h_\times = -\frac{4G\mathcal{M}}{c^2 D} \left(\frac{\pi G \mathcal{M} f}{c^3}\right)^{2/3} \cos \iota \, \sin 2\Phi_N(t), \tag{87}$$

where the phase

$$\Phi_N(t) = \int \Omega_{\rm orb} \, dt = \Phi_c - \left[\frac{c^3(t_c - t)}{5G\mathcal{M}}\right]^{5/8}. \tag{88}$$

The system's inclination ι is just the projection of its orbital angular momentum, $\mathbf{L}$, to the direction of propagation vector, $\mathbf{n}$: $\cos \iota = \hat{\mathbf{L}} \cdot \mathbf{n}$ (where $\hat{\mathbf{L}} = \mathbf{L}/|\mathbf{L}|$).

In later sections, we use Equation 87 as a reference to calibrate how effects we have neglected so far change the waves. Note that h_+ and $h_\times$ depend on, and thus encode, the chirp mass, the distance, the position on the sky (via the direction vector $\mathbf{n}$), and the orientation of the binary's orbital plane (via $\hat{\mathbf{L}}$).

3.4. Nonlinear Description of Waves

The nonlinear nature of GR is one of its most important defining characteristics. By linearizing, perhaps we are throwing out the baby with the bathwater, failing to characterize important aspects of gravitational radiation. Fortunately, we can derive a wave equation that fully encodes all nonlinear features of GR. This was apparently first derived by Penrose (1960); Ryan (1974) gives a very nice discussion of this equation's history and derivation. Begin by taking an additional derivative ∇^γ of the Bianchi identity (Equation 21), obtaining

$$\Box_g R_{\alpha\beta\mu\nu} = -\nabla^\gamma \nabla_\beta R_{\gamma\alpha\mu\nu} - \nabla^\gamma \nabla_\alpha R_{\beta\gamma\mu\nu}, \tag{89}$$

where $\Box_g \equiv g^{\gamma\delta} \nabla_\gamma \nabla_\delta$ is a covariant wave operator. Next, use the fact that the commutator of covariant derivatives generates the Riemann tensor:

$$[\nabla_\gamma, \nabla_\delta] p_\mu \equiv (\nabla_\gamma \nabla_\delta - \nabla_\delta \nabla_\gamma) p_\mu = -R^\sigma_{\mu\gamma\delta} p_\sigma, \tag{90}$$

$$[\nabla_\gamma, \nabla_\delta] p_{\mu\nu} = -R^\sigma_{\mu\gamma\delta} p_{\sigma\nu} - R^\sigma_{\nu\gamma\delta} p_{\mu\sigma}. \tag{91}$$

Extension to further indices is hopefully obvious. Manipulating Equation 89 yields a wave equation for Riemann in which (Riemann)^2 acts as the source term. This is the Penrose wave equation; see Ryan (1974) for more details.

If spacetime is vacuum [$T_{\mu\nu} = 0$, so that via the Einstein equation (Equation 29) $R_{\mu\nu} = 0$], the Penrose wave equation simplifies quite a bit, yielding

$$\Box_g R_{\alpha\beta\mu\nu} = 2 R_{\mu\sigma\beta\tau} R_{\nu\alpha}^{\sigma\tau} - 2 R_{\mu\sigma\alpha\tau} R_{\nu\beta}^{\sigma\tau} + R_{\mu\sigma\tau\sigma} R_{\alpha\beta}^{\tau\sigma}. \tag{92}$$

A variant of Equation 92 underlies much of black hole perturbation theory, our next topic.

4. PERTURBATION THEORY

Perturbation theory is the first technique we discuss for modeling strong-field merging compact binaries. The basic concept is to assume that the spacetime is an exact solution perturbed by a small orbiting body and to expand to first order in the binary's mass ratio. Some of the most interesting strong-field binaries have black holes, so we focus on black hole perturbation theory. Perturbation theory analysis of binaries has two important applications. First, it can be a limiting case of the pN expansion: Perturbation theory for binaries with separations $r \gg GM/c^2$ should give the same result as pN theory in the limit $\mu \ll M$. We return to this point in Section 5. Second, perturbation theory is an ideal tool for extreme mass ratio captures, binaries created by the scattering of a stellar mass ($m \sim 1 - 100\,M_\odot$) body onto a strong-field orbit of a massive ($M \sim 10^5 - 10^7\,M_\odot$) black hole.

4.1. Basic Concepts and Overview of Formalism

At its most basic, black hole perturbation theory is developed much like the weak gravity limit described in Section 3.1, replacing the flat spacetime metric $\eta_{\alpha\beta}$ with the spacetime of a black hole:

$$g_{\mu\nu} = g_{\mu\nu}^{\text{BH}} + h_{\mu\nu}. \tag{93}$$

For astrophysical scenarios, one uses the Schwarzschild (nonrotating black hole) or Kerr (rotating) solutions for $g_{\mu\nu}^{\text{BH}}$. It is straightforward (though somewhat tedious) to then develop the Einstein tensor for this spacetime, keeping terms only to first order in the perturbation h.

This approach works very well when the background is nonrotating,

$$(ds^2)^{\text{BH}} = g_{\mu\nu}^{\text{BH}} dx^\mu dx^\nu = -\left(1 - \frac{2\hat{M}}{r}\right) dt^2 + \frac{dr^2}{(1 - 2\hat{M}/r)} + r^2 d\Omega^2, \tag{94}$$

where $d\Omega^2 = d\theta^2 + \sin^2\theta d\phi^2$ and $\hat{M} = GM/c^2$. We consider this special case in detail; our discussion is adapted from Rezzolla (2003). Because the background is spherically symmetric, it is useful to decompose the perturbation into spherical harmonics. For example, under rotations in θ and ϕ, h_{00} should transform as a scalar. We thus put

$$h_{00} = \sum_{lm} a_{lm}(t, r) Y_{lm}(\theta, \phi). \tag{95}$$

The components h_{0i} transform like components of a three-vector under rotations and can be expanded in vector harmonics; h_{ij} can be expanded in tensor harmonics. One can decompose further with parity: Even harmonics acquire a factor $(-1)^l$ when $(\theta, \phi) \to (\pi - \theta, \phi + \pi)$; odd harmonics acquire a factor $(-1)^{l+1}$.

By imposing these decompositions, choosing a particular gauge, and requiring that the space-time satisfy the vacuum Einstein equation $G_{\mu\nu} = 0$, we find an equation that governs the perturbations. Somewhat remarkably, the t and r dependence for all components of $h_{\mu\nu}$ for given spherical harmonic indices (l, m) can be constructed from a function $Q(t, r)$ governed by the simple equation

$$\frac{\partial^2 Q}{\partial t^2} - \frac{\partial^2 Q}{\partial r_*^2} - V(r)Q = 0, \tag{96}$$

where $r_* = r + 2\hat{M} \ln(r/2\hat{M} - 1)$. The potential $V(r)$ depends on whether we consider even or odd perturbations:

$$V_{\text{even}}(r) = \left(1 - \frac{2\hat{M}}{r}\right)\left[\frac{2q(q+1)r^3 + 6q^2\hat{M}r^2 + 18q\hat{M}^2r + 18\hat{M}^3}{r^3(qr + 3\hat{M})^2}\right], \tag{97}$$

where $q = (l-1)(l+2)/2$, and

$$V_{\text{odd}}(r) = \left(1 - \frac{2\hat{M}}{r}\right)\left[\frac{l(l+1)}{r^2} - \frac{6\hat{M}}{r^3}\right]. \tag{98}$$

For even parity, Equation 96 is the Zerilli equation (Zerilli 1970); for odd parity, it is the Regge-Wheeler equation (Regge & Wheeler 1957). For further discussion, including how gauge is chosen and how to construct $h_{\mu\nu}$ from Q, see Rezzolla (2003). Finally, note that when the spacetime perturbation is due to a body orbiting the black hole, these equations acquire a source term. One can construct the full solution for the waves from an orbiting body by using the source-free equation to build a Green's function, and then integrating over that source.

How does this procedure fare for rotating holes? The background spacetime,

$$(ds^2)^{\text{BH}} = -\left(1 - \frac{2\hat{M}r}{\rho^2}\right)dt^2 - \frac{4a\hat{M}r\sin^2\theta}{\rho^2}dtd\phi + \frac{\rho^2}{\Delta}dr^2 + \rho^2 d\theta^2$$
$$+ \left(r^2 + a^2 + \frac{2\hat{M}ra^2\sin^2\theta}{\rho^2}\right)d\phi^2, \tag{99}$$

where

$$a = \frac{|\vec{S}|}{cM}, \quad \rho^2 = r^2 + a^2\cos^2\theta, \quad \Delta = r^2 - 2\hat{M}r + a^2, \tag{100}$$

is now markedly nonspherical. (We have used Boyer-Lindquist coordinates, but the nonspherical nature is independent of coordinate choice.) So, the decomposition into spherical harmonics is not useful. One could, in principle, simply expand $G_{\mu\nu} = 0$ to first order in $h_{\mu\nu}$ and obtain a partial differential equation in t, r, and θ. (The metric is axially symmetric, so we can easily separate the ϕ dependence.) This author is unaware of such a formulation. One issue is that the gauge used for the perturbation must be specified; this may be complicated in the general case. More important historically, the equations so developed do not appear to separate. As we see in a moment, a different approach does yield separable equations, which were preferred for much of the history of this field.

Rather than expanding the metric of the black hole, Teukolsky (1973) examined perturbations of its curvature:

$$R_{\alpha\mu\beta\nu} = R_{\alpha\mu\beta\nu}^{\text{BH}} + \delta R_{\alpha\mu\beta\nu}. \tag{101}$$

The curvature tensor is invariant to first-order gauge transformations, an attractive feature. This tensor also obeys the nonlinear wave equation (Equation 92). By expanding that equation to linear

order in $\delta R_{\alpha\mu\beta\nu}$, Teukolsky showed that perturbations to Kerr black holes are governed by the equation

$$
\left[\frac{(r^2 + a^2)^2}{\Delta} - a^2 \sin^2\theta \right] \partial_t^2 \Psi - 4 \left[r + ia\cos\theta - \frac{\hat{M}(r^2 - a^2)}{\Delta} \right] \partial_t \Psi
$$

$$
+ \frac{4i\hat{M}amr}{\Delta} \partial_t \Psi - \Delta^2 \partial_r \left(\Delta^{-1} \partial_r \Psi \right) - \frac{1}{\sin\theta} \partial_\theta \left(\sin\theta\, \partial_\theta \Psi \right) \tag{102}
$$

$$
- \left[\frac{a^2}{\Delta} - \frac{1}{\sin^2\theta} \right] m^2 \Psi + 4im \left[\frac{a(r - \hat{M})}{\Delta} + \frac{i\cos\theta}{\sin^2\theta} \right] \Psi - \left(4\cot^2\theta + 2 \right) \Psi = \mathcal{T}.
$$

Ψ is a complex quantity built from a combination of components of $\delta R_{\alpha\mu\beta\nu}$ and describes space-time's radiation; see Teukolsky (1973) for details. (We have assumed $\Psi \propto e^{im\phi}$.) Likewise, $\mathcal{T}$ describes a source function built from the stress-energy tensor describing a small body orbiting the black hole. Somewhat amazingly, Equation 102 separates; putting

$$
\Psi = \int d\omega \sum_{lm} R_{lm}(r) S_{lm}(\theta) e^{im\phi - i\omega t} \tag{103}
$$

and applying a similar decomposition to the source $\mathcal{T}$, we find that $S(\theta)$ is a spin-weighted spheroidal harmonic (a basis for tensor functions in a nonspherical background), and that $R(r)$ is governed by a simple ordinary differential equation. Ψ characterizes Kerr perturbations in much the same way that Q (cf. Equation 96) characterizes them for Schwarzschild.

Whether one uses this separation or solves Equation 102 directly, solving for perturbations of black holes is now a well-understood enterprise. We now discuss how one uses these solutions to model compact binaries.

4.2. Binary Evolution in Perturbation Theory

How do we describe the motion of a small body about a black hole? The most rigorous approach is to enforce $\nabla^\mu T_{\mu\nu} = 0$, where $T_{\mu\nu}$ describes the small body in the spacetime of the large black hole. If we neglect the small body's perturbation to the spacetime, this exercise produces the geodesic equation $u^\mu \nabla_\mu u^\nu = 0$, where u^μ is the small body's four-velocity. Geodesic black hole orbits have been studied extensively; see, for example, Misner, Thorne & Wheeler (1973, chapter 33). A key feature of these orbits is that they are characterized (up to initial conditions) by three conserved constants: energy E, axial angular momentum L_z, and Carter's constant Q. If the black hole does not rotate, Carter's constant is related to the orbit's total angular momentum: $Q(a = 0) = \mathbf{L} \cdot \mathbf{L} - L_z^2$. When the black hole rotates rapidly, Q is not so easy to interpret, but the idea that it is essentially the rest of the orbit's angular momentum can be useful.

Now take into account perturbations from the small body. Enforcing $\nabla^\mu T_{\mu\nu} = 0$, we find that the small body follows a forced geodesic,

$$
u^\mu \hat{\nabla}_\mu u^\nu = f^\nu, \tag{104}
$$

where $\hat{\nabla}_\mu$ is the covariant derivative in the background black-hole spacetime. The novel feature of Equation 104 is the self force f^ν, a correction to the motion of order the small body's spacetime perturbation. The self force is so named because it arises from the body's interaction with its own spacetime correction.

Self forces have a long pedigree. Dirac (1938) showed that a self force arises from the back-reaction of an electromagnetic charge on itself and causes radiative damping. Computing the gravitational self force near a black hole is an active area of current research. It is useful to break

the self force into a dissipative piece, f_{diss}^{ν}, which is asymmetric under time reversal, and a conservative piece, f_{cons}^{ν}, which is symmetric. These contributions have very different impact on the orbit. Dissipation causes the conserved quantities (E, L_z, Q) to decay, driving inspiral of the small body. Quinn & Wald (1999) have shown that the rate at which E and L_z change due to f_{diss}^{ν} is identical to what is found when one computes the fluxes of energy and angular momentum encoded by the Isaacson tensor (71).

The conservative self force, by contrast, does not cause orbit decay. Conserved constants are still conserved when we include this force; but the orbits are different from background geodesics. This reflects the fact that, even neglecting dissipation, the small body's motion is determined by the full spacetime, not just the background black hole. When conservative effects are taken into account, one finds that the orbital frequencies are shifted by an amount

$$\delta\Omega_x \sim \Omega_x \times (\mu/M) \tag{105}$$

[where $x \in (\phi, \theta, r)$]. Because the GWs have spectral support at harmonics of the orbital frequencies, these small but nonnegligible frequency shifts are directly encoded in the waves that the binary generates. Good discussion and a toy model can be found in Pound, Poisson & Nickel (2005).

To date, not a large amount of work is published regarding self forces and conservative effects for Kerr orbits. There has, however, been enormous progress for the case of orbits around nonrotating holes. Barack & Sago (2007) have completed an analysis of the full self force for circular orbits about a Schwarzschild black hole; generalization to eccentric orbits is in progress (L. Barack, private communication). An independent approach developed by Detweiler (2008) has been found to agree with Barack & Sago extremely well; see Sago, Barack & Detweiler (2008) for detailed discussion of this comparison.

4.3. Gravitational Waves from Extreme Mass Ratio Binaries

In this section, we discuss the properties of GWs and GW sources as calculated using perturbation theory. As discussed in Section 1.3, these waves most naturally describe extreme mass ratio capture sources. There is also an important overlap with the pN results discussed in Section 5: By specializing to circular, equatorial orbits and considering the limit $r \gg GM/c^2$, results from perturbation theory agree with pN results for $\mu/M \ll 1$.

Our goal here is to highlight features of the generic Kerr inspiral waveform. As such, we neglect the conservative self force, which is not yet understood for the Kerr case well enough to be applied to these waves. When conservative effects are neglected, the binary can be regarded as evolving through a sequence of geodesics, with the sequence determined by the rates at which GWs change the constants E, L_z, and Q. Modeling compact binaries in this limit takes three ingredients: first, a description of black hole orbits; second, an algorithm to compute GWs from the orbits and to infer how the waves' backreaction evolves us from orbit to orbit; and third, a method to integrate along the orbital sequence to build the full waveform. A description of this method is given by Hughes et al. (2005); we summarize the main results of these three ingredients here.

4.3.1. Black hole orbits. Motion in the vicinity of a black hole can be conveniently written in the Boyer-Lindquist coordinates of Equation 99 as $r(t)$, $\theta(t)$, and $\phi(t)$. Because t corresponds to time far from the black hole, this gives a useful description of the motion as measured by distant observers. Bound black hole orbits are confined to a region near the hole. They have $r_{\min} \le r(t) \le r_{\max}$ and $\theta_{\min} \le \theta(t) \le \pi - \theta_{\min}$. Bound orbits thus occupy a torus in the three-space near the hole's event horizon; an example is shown in **Figure 1**, taken from Drasco & Hughes (2006). Selecting the
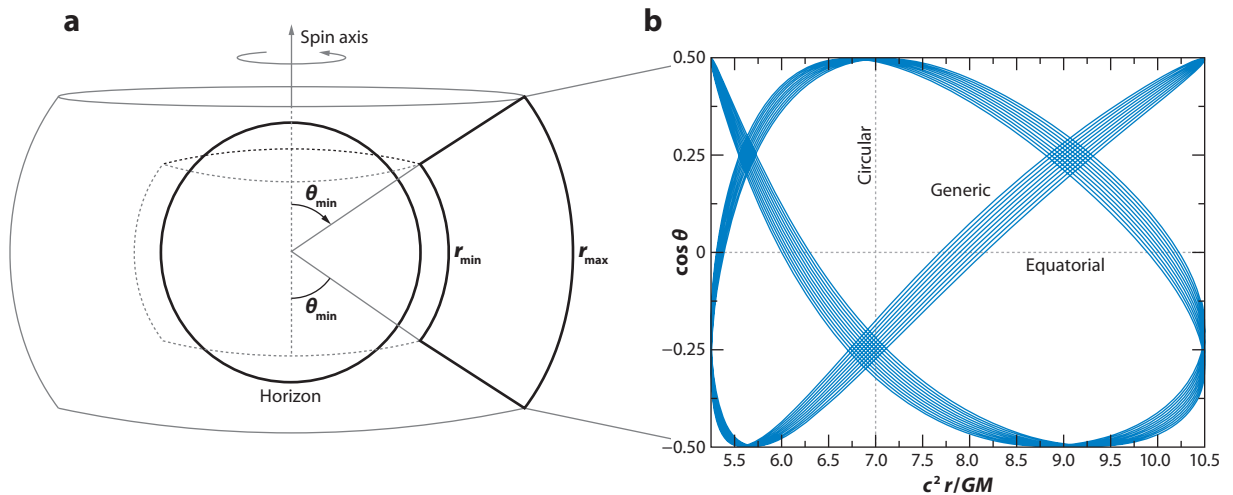
Figure 1

The geometry of a generic Kerr black hole orbit (taken from Drasco & Hughes 2006). This orbit is about a black hole with spin parameter $a = 0.998\,M$. The range of its radial motion is determined by $p = 7GM/c^2$ and $e = 1/3$; θ ranges from 60° to 120°. (*a*) The torus in the coordinate space this torus occupies. (*b*) How a generic orbit ergodically fills this torus.

orbital constants E, L_z, and Q fully determines $r_{\min/\max}$ and $\theta_{\min}$. It is useful for some discussions to reparameterize the radial motion, defining an eccentricity e and a semilatus rectum p via

$$r_{\min} = \frac{p}{1+e}, \quad r_{\max} = \frac{p}{1-e}. \tag{106}$$

For many bound black hole orbits, $r(t)$, $\theta(t)$, and $\phi(t)$ are periodic (Schmidt 2002; see also Drasco & Hughes 2004). (Exceptions are orbits that plunge into the black hole; we discuss these below.) Near the hole, the time to cover the r range becomes distinct from the time to cover the θ range, which becomes distinct from the time to cover 2π radians of azimuth. One can say that spacetime curvature splits the Keplerian orbital frequency Ω into Ω_r, Ω_θ, and Ω_ϕ. **Figure 2** shows these three frequencies, plotted as functions of semimajor axis A for fixed values of e and $\theta_{\min}$. Notice that all three approach $\Omega \propto A^{-3/2}$ for large A.

4.3.2. Gravitational radiation from orbits. Because their orbits are periodic, GWs from a body orbiting a black hole have support at harmonics of the orbital frequencies. One can write the two polarizations as

$$h_+ + ih_\times = \sum H_{mkn} e^{i\omega_{mkn} t}, \quad \text{where} \tag{107}$$

$$\omega_{mkn} = m\Omega_\phi + k\Omega_\theta + n\Omega_r. \tag{108}$$

The amplitude H_{mkn} can be found by solving the Teukolsky equation (Equation 102) using the decomposition (Equation 103); details for the general case are given by Drasco & Hughes (2006). An example of a wave from a geodesic orbit is shown in **Figure 3**. Note the different timescales apparent in this wave that are due to the three distinct frequencies of the underlying geodesic orbit (and their harmonics).

The expansion (Equation 107) does not work well for orbits that plunge into the black hole; those orbits are not periodic and cannot be expanded using a set of real frequencies. A better way to calculate those waves is to solve the Teukolsky equation (Equation 102) without introducing

a = 0.998 M
e = 0.5
θ_{min} = 75°
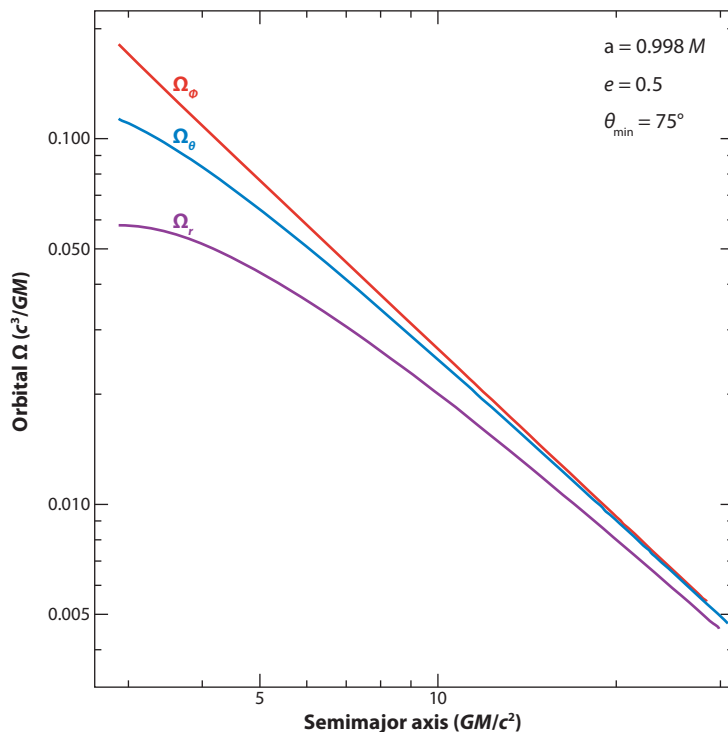
Figure 2

Orbital frequencies for generic Kerr black hole orbits. We vary the orbits' semilatus rectum p, but fix eccentricity $e = 0.5$ and inclination parameter $\theta_{min} = 75°$. Our results are plotted as a function of semimajor axis $A = p/\sqrt{1 - e^2}$. All three frequencies asymptote to the Keplerian value $\Omega = \sqrt{GM/A^3}$ in the weak field, but differ significantly from each other in the strong field.

the decomposition (Equation 103). Results for waves from plunging orbits in the language of perturbation theory were first given by Nagar, Damour & Tartaglia (2007); Sundararajan (2008) has recently extended the cases that we can model to full generality.

As mentioned in Section 4.2, it is fairly simple to compute the flux of energy $\dot{E}$ and angular momentum $\dot{L}_z$ from the Isaacson tensor, Equation 71, once the waves are known. Recent work (Ganz et al. 2007) has shown that a similar result describes $\dot{Q}$. Once $\dot{E}$, $\dot{L}_z$, and $\dot{Q}$ are known, it is straightforward to evolve the orbital elements $r_{min/max}$ and θ_{min}, specifying the sequence of orbits through which gravitational radiation drives the system. **Figure 4** gives an example of how orbits evolve when their eccentricity is zero.

4.3.3. Evolving through an orbital sequence. It is not too difficult to compute the sequence of orbits [parameterized as $E(t)$, $L_z(t)$, $Q(t)$ or $r_{min/max}(t)$, $\theta_{min}(t)$] that an inspiraling body passes through before finally plunging into its companion black hole. Once these are known, it is straightforward to build the worldline that a small body follows as it spirals into the black hole. From the worldline, we can build a source function $\mathcal{T}(t)$ for Equation 102 and compute the evolving inspiral waves. **Figure 5** gives an example of a wave arising from the inspiral of a small body into a black hole; see Sundararajan et al. (2008) for details of how these waves are computed.
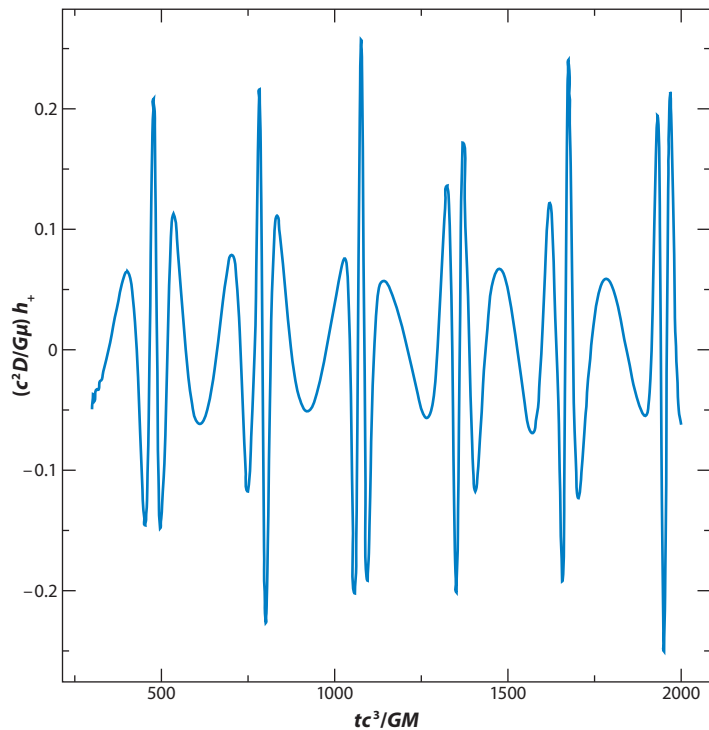
Figure 3

Waveform arising from a generic geodesic black hole orbit, neglecting orbital evolution due to backreaction. This orbit has $p = 8GM/c^2$ and $e = 0.5$, corresponding to motion in the range of $16GM/3c^2 \leq r(t) \leq 16GM/c^2$; it also has $\theta_{\min} = 60°$. The large black hole has a spin parameter $a = 0.9M$. Note that the wave has structure at several timescales, corresponding to the three frequencies Ω_r, Ω_θ, and Ω_ϕ (cf. **Figure 2**).

5. POST-NEWTONIAN THEORY

Suppose we cannot use mass ratio as an expansion parameter. For instance, if the members of the binary are of equal mass, then $\eta \equiv m_1 m_2/(m_1 + m_2)^2 = 0.25$. This is large enough that neglect of $\mathcal{O}(\eta^2)$ and higher terms is problematic. The techniques discussed in Section 4 are not appropriate.

If the mass ratio is not a good expansion parameter, the potential $\phi \equiv GM/rc^2$ may be. The pN expansion of GR results when we use ϕ as our expansion parameter. We now summarize the main concepts that underlie the pN formalism, turning next to a discussion of the pN waveform and its interesting features. Much of our discussion is based on Blanchet (2006).

5.1. Basic Concepts and Overview of Formalism

One typically begins the pN expansion by examining the Einstein field equations in harmonic or de Donder coordinates (e.g., Weinberg 1972, section 7.4). In these coordinates, one defines

$$h^{\mu\nu} \equiv \sqrt{-g}g^{\mu\nu} - \eta^{\mu\nu}, \tag{109}$$

where g is the determinant of $g_{\mu\nu}$. This looks similar to the flat spacetime perturbation defined in Section 3.1; however, we do not assume that h is small. We next impose the gauge
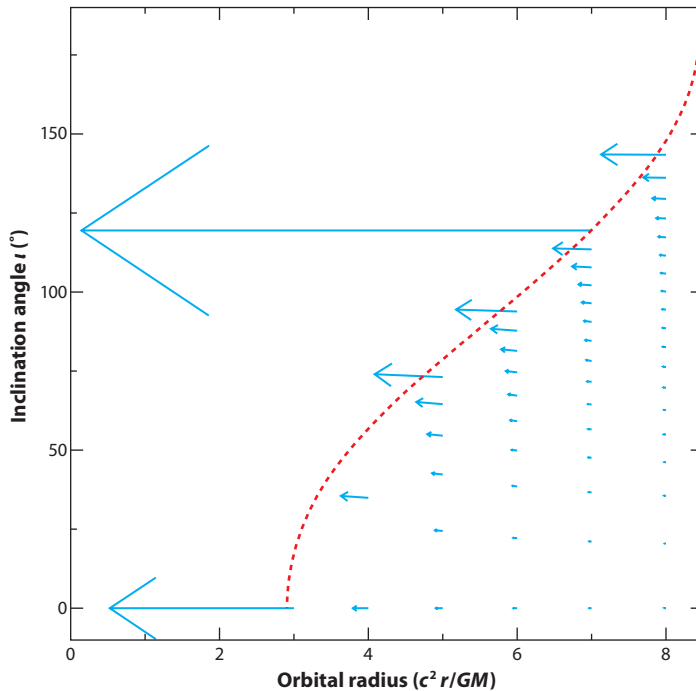
Figure 4

The evolution of circular orbits ($e = 0$) about a black hole with $a = 0.8\,M$; taken from Hughes (2000). The inclination angle ι is given by $\iota \simeq \pi/2 - \theta_{\min}$; the equality is exact for $\theta_{\min} = 0$ and for $a = 0$. In the general case, this relation misestimates ι by $\lesssim 3\%$; see Hughes (2000) for detailed discussion. The dotted line is this hole's last stable orbit; orbits to the left are unstable to small perturbations, whereas those to the right are stable. Each arrow shows how radiation tends to evolve an orbit; length indicates how strongly it is driven. These orbits are driven to smaller radius and to (very slightly) larger inclination. The extremely long arrow at $\iota \simeq 120°$, $r = 7GM/c^2$ lies very close to the last stable orbit. As such, a small push from radiation has a large impact.

condition

$$\partial_\alpha b^{\alpha\beta} = 0. \tag{110}$$

With these definitions, the exact Einstein field equation is

$$\Box b^{\alpha\beta} = \frac{16\pi\,G}{c^4}\tau^{\alpha\beta}, \tag{111}$$

where $\Box = \eta^{\alpha\beta}\partial_\alpha\partial_\beta$ is the flat spacetime wave operator. The form of Equation 111 means that the radiative Green's function we used to derive Equation 40 can be applied here as well; the solution is simply

$$b^{\alpha\beta} = -\frac{4G}{c^4}\int \frac{\tau_{\alpha\beta}(\mathbf{x}', t - |\mathbf{x} - \mathbf{x}'|/c)}{|\mathbf{x} - \mathbf{x}'|}d^3x'. \tag{112}$$

Formally, Equation 112 is exact. We have swept some crucial details under the rug, however. In particular, we never defined the source $\tau^{\alpha\beta}$. It is given by

$$\tau^{\alpha\beta} = (-g)T^{\alpha\beta} + \frac{c^4\Lambda^{\alpha\beta}}{16\pi\,G}, \tag{113}$$
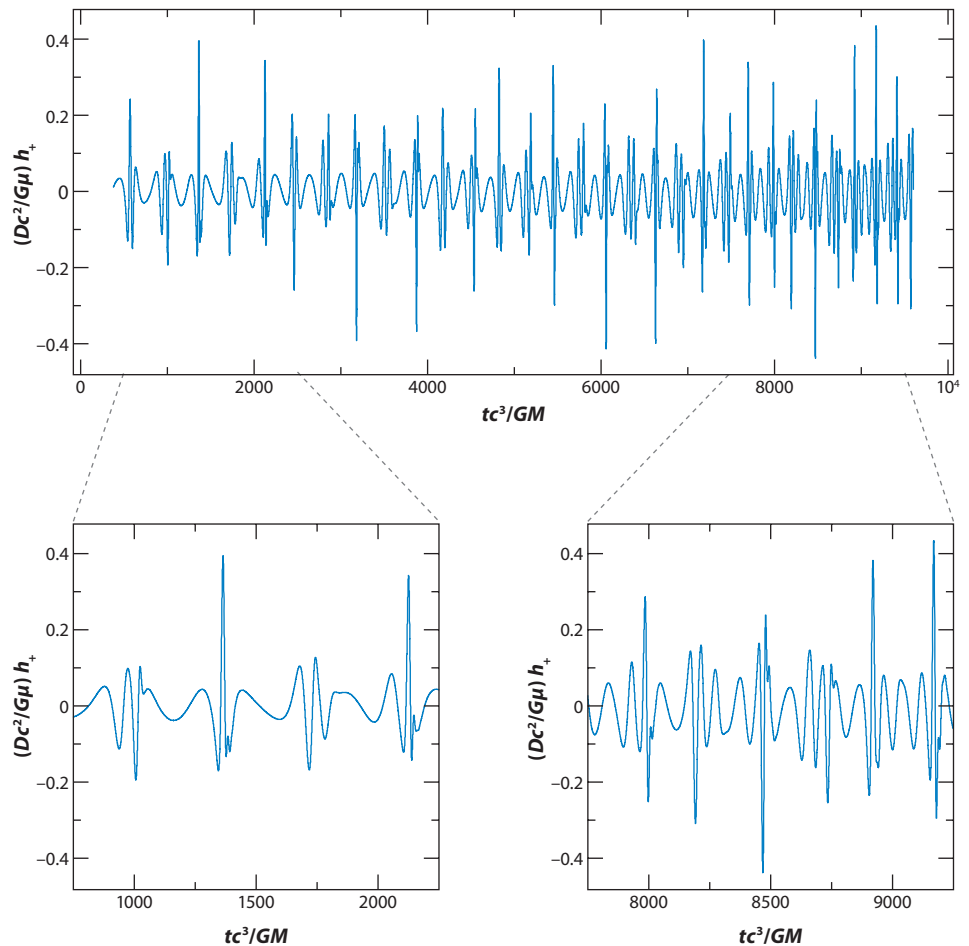
Figure 5

Plus polarization of wave generated by a small body spiraling into a massive black hole; this figure is adapted from Sundararajan et al. (2008). The amplitude is scaled to the source's distance D and the small body's mass μ; time is measured in units c^3/GM. For this calculation, the binary's initial parameters are $p = 10GM/c^2$, $e = 0.5$, and $\theta_{\min} \simeq 61°$; the binary's mass ratio is fixed to $\mu/M = 0.016$, and the larger black hole's spin parameter is $a = 0.5M$. The insets show spans of length $\Delta t \sim 1000GM/c^3$ early and late in the inspiral. Note the substantial evolution of the wave's frequencies as the orbital shrinks.

where $T^{\alpha\beta}$ is the usual stress energy tensor, and $\Lambda^{\alpha\beta}$ encodes much of the nonlinear structure of the Einstein field equations:

$$\Lambda^{\alpha\beta} \equiv 16\pi(-g)t_{LL}^{\alpha\beta} + \partial_\nu h^{\alpha\mu}\partial_\mu h^{\beta\nu} - \partial_\mu\partial_\nu h^{\alpha\beta}h^{\mu\nu} \tag{114}$$

$$= N^{\alpha\beta}[h, h] + M^{\alpha\beta}[h, h, h] + L^{\alpha\beta}[h, h, h, h] + \mathcal{O}(h^5). \tag{115}$$

On the first line, $t_{LL}^{\alpha\beta}$ is the Landau-Lifshitz pseudotensor, a quantity that (in certain gauges) allows us to describe how GWs carry energy through spacetime (Landau & Lifshitz 1975, Section 96); on the second line, the term $N^{\alpha\beta}[h, h]$ means a collection of terms quadratic in h and its derivatives; $M^{\alpha\beta}[h, h, h]$ is a cubic term, etc. Our solution $h^{\alpha\beta}$ appears on both the left- and right-hand sides of Equation 112. Such a structure can be handled very well iteratively.

We write

$$b^{\alpha\beta} = \sum_{n=1}^{\infty} G^n b_n^{\alpha\beta}. \tag{116}$$

The $n = 1$ term is essentially the linearized solution from Section 3.1. To go higher, let $\Lambda_n^{\alpha\beta}$ denote the contribution of $\Lambda^{\alpha\beta}$ to the solution $b_n^{\alpha\beta}$. We find

$$\Lambda_2^{\alpha\beta} = N^{\alpha\beta}[b_1, b_1], \tag{117}$$

$$\Lambda_3^{\alpha\beta} = M^{\alpha\beta}[b_1, b_1, b_1] + N^{\alpha\beta}[b_2, b_1] + N^{\alpha\beta}[b_1, b_2], \tag{118}$$

etc.; higher contributions to Λ^{ab} can be found by expanding its definition and gathering terms. By solving the equations that result from this procedure, it becomes possible to build the spacetime metric and describe the motion of the members of a binary and the radiation that they emit.

5.2. Features of the Post-Newtonian Binary Waveform

The features of the pN binary waveform are most naturally understood by first considering how we describe the motion of the members of the binary. Take those members to have masses m_1 and m_2, let their separation be r, and let $\mathbf{r}$ point to body 1 from body 2. Then, in the harmonic gauge used for pN theory, the acceleration of body 1 due to the gravity of body 2 is

$$\mathbf{a} = \mathbf{a}_0 + \mathbf{a}_2 + \mathbf{a}_4 + \mathbf{a}_5 + \mathbf{a}_6 + \mathbf{a}_7 \dots. \tag{119}$$

The zeroth term,

$$\mathbf{a}_0 = -\frac{Gm_2}{r^2}\mathbf{r}, \tag{120}$$

is just the usual Newtonian gravitational acceleration. Each $\mathbf{a}_n$ is a pN correction of order $(v/c)^n$. The first such correction is

$$\mathbf{a}_2 = \left\{ \frac{5G^2 m_1 m_2}{r^3} + \frac{4G^2 m_2^2}{r^3} + \frac{Gm_2}{r^2} \left[\frac{3}{2}(\mathbf{r} \cdot \mathbf{v}_2)^2 - v_1^2 + 4\mathbf{v}_1 \cdot \mathbf{v}_2 - 2v_2^2 \right] \right\} \frac{\mathbf{r}}{c^2}. \tag{121}$$

For the acceleration of body 2 due to body 1, exchange labels 1 and 2 and replace $\mathbf{r}$ with $-\mathbf{r}$. Note that $\mathbf{a}_2$ changes the dependence of the acceleration with respect to orbital separation. It also shows that the acceleration of body 1 depends on its mass m_1. This is a pN manifestation of the self force discussed in Section 4.2. So far, the pN acceleration has been computed to order $(v/c)^7$. As we go to high order, the expressions for $\mathbf{a}_n$ become quite lengthy. An excellent summary is given by Blanchet (2006, their equation 131 and surrounding text; note that the expression for $\mathbf{a}_6$ fills over two pages in that paper!).

At higher order, we also find a distinctly non-Newtonian element to binary dynamics: Its members spins precess owing to their motion in the binary's curved spacetime. If the spins are $\mathbf{S}_1$ and $\mathbf{S}_2$, one finds (Thorne & Hartle 1985)

$$\frac{d\mathbf{S}_1}{dt} = \frac{G}{c^2 r^3} \left[\left(2 + \frac{3}{2}\frac{m_2}{m_1} \right) \mu\sqrt{Mr}\hat{\mathbf{L}} \right] \times \mathbf{S}_1 + \frac{G}{c^2 r^3} \left[\frac{1}{2}\mathbf{S}_2 - \frac{3}{2}(\mathbf{S}_2 \cdot \hat{\mathbf{L}})\hat{\mathbf{L}} \right] \times \mathbf{S}_1, \tag{122}$$

and

$$\frac{d\mathbf{S}_2}{dt} = \frac{G}{c^2 r^3} \left[\left(2 + \frac{3}{2}\frac{m_1}{m_2} \right) \mu\sqrt{Mr}\hat{\mathbf{L}} \right] \times \mathbf{S}_2 + \frac{G}{c^2 r^3} \left[\frac{1}{2}\mathbf{S}_1 - \frac{3}{2}(\mathbf{S}_1 \cdot \hat{\mathbf{L}})\hat{\mathbf{L}} \right] \times \mathbf{S}_2. \tag{123}$$

We now discuss the ways in which aspects of pN binary dynamics color a system's waves.

5.2.1. Gravitational-wave amplitudes. Although a binary's dominant waves come from variations in its mass quadrupole moment, Equation 53 shows us that higher moments also generate

Figure 6

The first three contributions to the + GW polarization, and their sum. In all panels, we plot $(Dc^2/G\mu)h_+$ versus tc^3/GM. Panel *a* gives the sum (cf. Equation 124) arising from H_+^0, $H_+^{1/2}$, and H_+^1; panels *b–d* show the individual contributions from those H_+^n. Although subdominant, the terms other than H_+^0 make a substantial contribution to the total, especially at the end of inspiral (here normalized to $c^3t/GM = 1$).
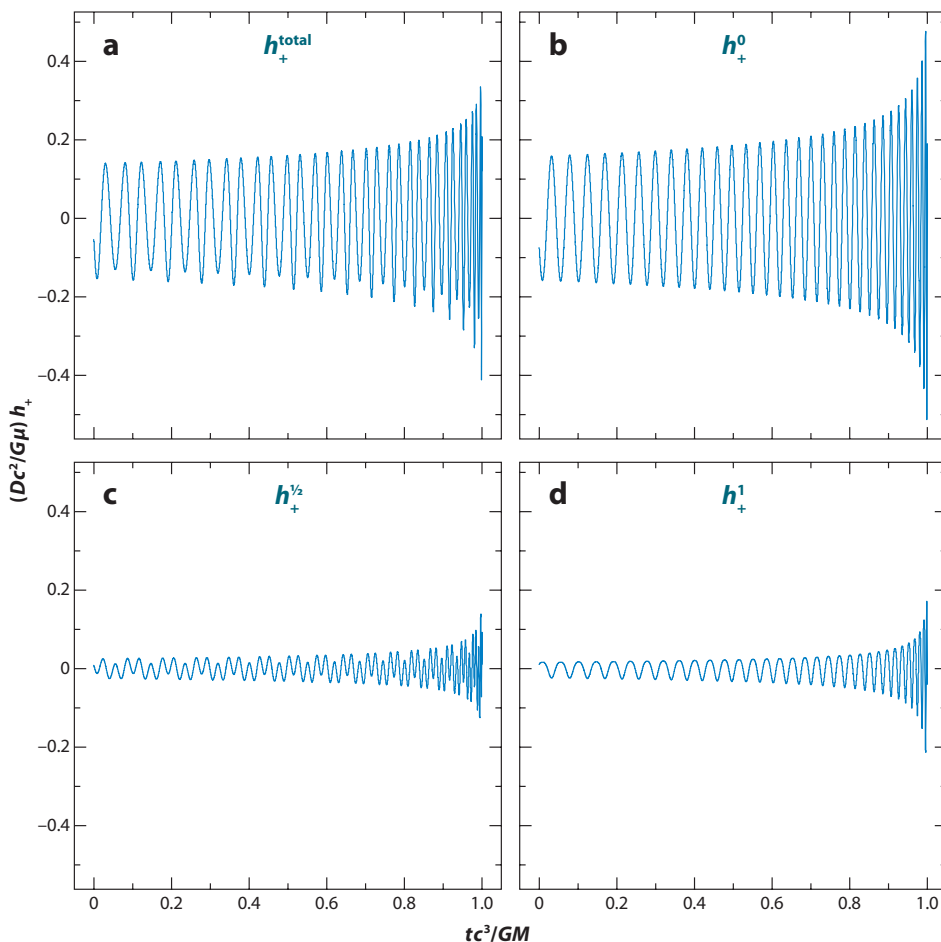
GWs. In the pN framework, these moments contribute to the amplitude of a binary's waves beyond the quadrupole formula (Equation 87). Write the gravitational waveform from a source as

$$ h_{+,\times} = \frac{2G\mathcal{M}}{c^2 D} \left(\frac{\pi G \mathcal{M} f}{c^3} \right)^{2/3} \left[H_{+,\times}^0 + v^{1/2} H_{+,\times}^{1/2} + v H_{+,\times}^1 + \cdots \right], \tag{124} $$

where $v \equiv (\pi GMf/c^3)^{1/3}$ is roughly the orbital speed of the binary's members (normalized to c). The contributions H_+^0 and $H_\times^0$ will reproduce the waveform presented in Equation 87. The higher-order terms $H_{+,\times}^{1/2}$ can be found in Blanchet (2006), his equations 237 through 241. For our purposes, the key point to note is that these higher-order terms introduce new dependences on the binary's orbital inclination and its masses. As such, measurement of these terms can provide additional constraints to help us understand the system's characteristics. **Figure 6** illustrates the three contributions H^0, $H^{1/2}$, and H^1 to the waves.

5.2.2. Orbital phase. The motion of a binary's members about each other determines the orbital phase. Specializing to circular orbits, we can determine the orbital frequency from the acceleration of the binary's members; integrating up this frequency, we define the binary's phase $\Phi(t)$. The first

few terms of this phase are given by Blanchet et al. (1995):

$$\Phi = \Phi_c - \left[\frac{c^3(t_c - t)}{5G\mathcal{M}}\right]^{5/8} \left[1 + \left(\frac{3715}{8064} + \frac{55}{96}\frac{\mu}{M}\right)\Theta^{-1/4} - \frac{3}{16}\left[4\pi - \beta(t)\right]\Theta^{-3/8}\right.$$
$$\left. + \left(\frac{9275495}{14450688} + \frac{284875}{258048}\frac{\mu}{M} + \frac{1855}{2048}\frac{\mu^2}{M^2} + \frac{15}{64}\sigma(t)\right)\Theta^{-1/2}\right],$$

(132)

where

$$\Theta = \frac{c^3\eta}{5GM}(t_c - t).$$

(133)

Notice that the leading term is just the Newtonian quadrupole phase (Equation 88). Each power of Θ connects to a higher order in the pN expansion; Equation 132 is taken to second pN order, which means that corrections of $(v/c)^4$ are included. Corrections to order $(v/c)^6$ are summarized by Blanchet (2006). In addition to the chirp mass $\mathcal{M}$ (which was defined immediately after Equation 81), the reduced mass μ enters Φ when higher-order terms are included. The high pN terms encode additional information about the binary's masses. At least in principle, including higher pN effects in our wave model makes it possible to determine both chirp mass and reduced mass, fully constraining the binary's masses.

Equation 132 also depends on two parameters, β and σ, which come from the binary's spins and orbit orientation. The spin-orbit parameter β is

$$\beta = \frac{1}{2}\sum_{i=1}^{2}\left[113\left(\frac{m_i}{M}\right)^2 + 75\eta\right]\frac{\mathbf{L}\cdot\mathbf{S}_i}{m_i^2};$$

(134)

the spin-spin parameter σ is

$$\sigma = \frac{\eta}{48m_1^2m_2^2}\left[721(\hat{\mathbf{L}}\cdot\mathbf{S}_1)(\hat{\mathbf{L}}\cdot\mathbf{S}_2) - 247\mathbf{S}_1\cdot\mathbf{S}_2\right]$$

(135)

(Blanchet et al. 1995). As we see in Section 8, these parameters encode valuable information, especially when spin precession is taken into account.

The $\mu \ll M$ limit of Equation 132 can be computed with black hole perturbation theory (Section 4) evaluated for circular orbits with $r \gg GM/c^2$. The orbital phase is found by integrating the orbital frequency. By changing variables, one can relate this to the orbital energy and the rate at which GWs evolve this energy:

$$\Phi = \int \Omega^{\text{orb}}\,dt = \int \frac{dE^{\text{orb}}/d\Omega}{dE^{\text{GW}}/dt}\Omega\,d\Omega.$$

(136)

The orbital energy E^{orb} is simple to calculate and to express as a function of orbital frequency. For example, for orbits of nonrotating black holes, we have

$$E^{\text{orb}} = \mu c^2\frac{1 - 2v^2/c^2}{\sqrt{1 - 3v^2/c^2}},$$

(137)

where $v \equiv r\Omega$. For circular, equatorial orbits, Mino et al. (1997) analytically solve the Teukolsky equation as an expansion in v, calculating dE^{GW}/dt to $\mathcal{O}[(v/c)^{11}]$. This body of work confirms, in a completely independent way, all of the terms that do not depend on the mass ratio μ/M in Equation 132. The fact that these terms are known to such high order is an important input to the effective one-body approach described in Section 5.3.

5.2.3. Spin precession. Although the spin vectors $\mathbf{S}_1$ and $\mathbf{S}_2$ wiggle around according to the prescription of Equations 122 and 123, the system must preserve a notion of global angular

momentum. Neglecting for a moment the secular evolution of the binary's orbit due to GW emission, pN theory teaches us that the total angular momentum

$$\mathbf{J} = \mathbf{L} + \mathbf{S}_1 + \mathbf{S}_2 \tag{138}$$

must be conserved. This means $\mathbf{L}$ must oscillate to compensate for the spins' dynamics and guarantees that, when spin precession is accounted for in our evolutionary models, the phase parameters β and σ become time varying. Likewise, the inclination angle ι varies with time. Precession thus leads to phase and amplitude modulation of a source's GWs. **Figure 7** illustrates precession's impact, showing the late inspiral waves for binaries that are identical aside from spin.
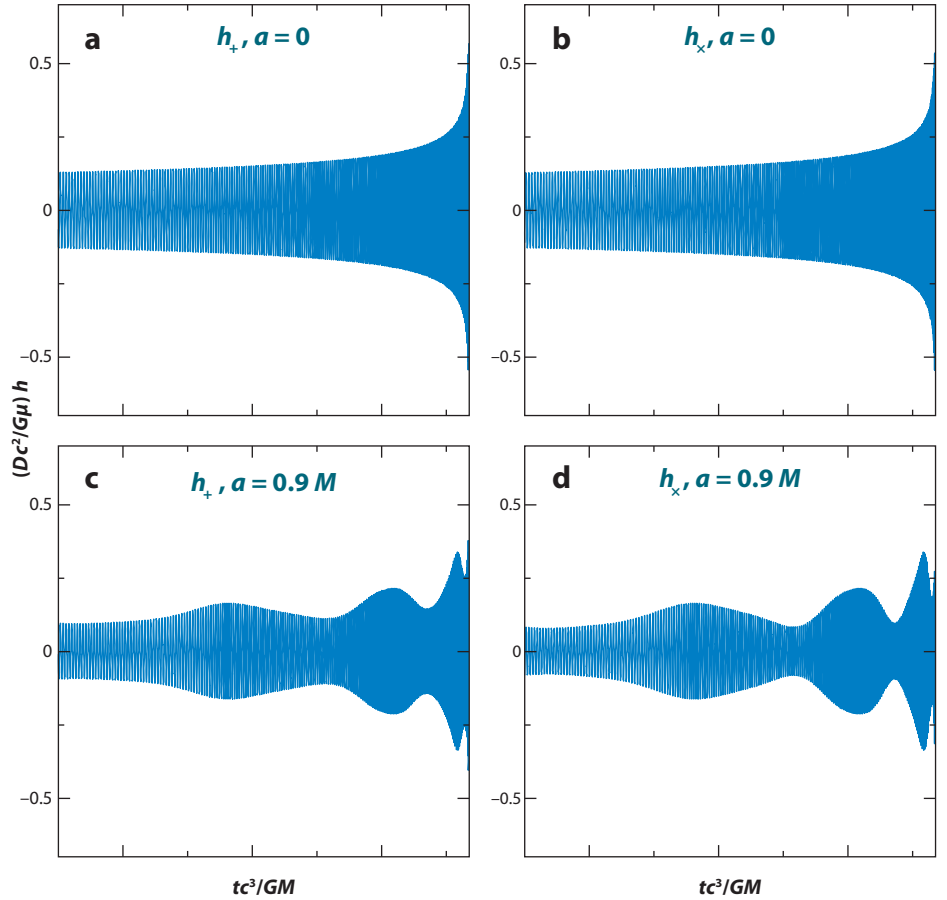
Figure 7

Illustration of precession's impact on a binary's waves. The top panels show h_+ and $h_\times$ for a binary that contains nonspinning black holes; the lower panels show the waveforms for a binary with rapid rapidly rotating ($a = 0.9M$) holes. The strong amplitude modulation is readily apparent in this figure. Less obvious, but also included, is the frequency modulation that enters through the spin-dependent orbital phase parameters β and σ (cf. Equation 132).

5.3. The Effective One-Body Approach

Since pN techniques are based on an expansion in $\phi = GM/rc^2$, it had been thought that they would only apply for $r \gtrsim 12 GM/c^2$ and that numerical relativity would be needed to cover the inspiral past that radius, through the final plunge and merger. This thinking was radically changed by Buonanno & Damour (1999), which introduced the effective one-body approach to two-body dynamics. This technique has proved to be an excellent tool for describing the late inspiral, plunge, and merger of two black holes. We now describe the key ideas of this approach; our description owes much to the helpful introductory lectures by Damour (2008).

As the name suggests, the key observation of this approach is that the motion of two bodies (m_1, m_2) about one another can be regarded as the motion of a single test body of mass $\mu = m_1 m_2 / (m_1 + m_2)$ in some spacetime. One begins by examining the Hamiltonian that gives the conservative contribution to the equations of motion. Let the binary's momenta be $\mathbf{p}_{1,2}$ and its generalized positions $\mathbf{q}_{1,2}$. If we work in the center of mass frame, then the Hamiltonian can only be a function of the relative position, $\mathbf{q} \equiv \mathbf{q}_1 - \mathbf{q}_2$, and can only depend on the momentum $\mathbf{p} \equiv \mathbf{p}_1 = -\mathbf{p}_2$. For example, the conservative motion can be described to second-pN order [i.e., $\mathcal{O}(v^4/c^4)$] with the Hamiltonian

$$H(\mathbf{q}, \mathbf{p}) = H_0(\mathbf{p}, \mathbf{q}) + \frac{1}{c^2} H_2(\mathbf{p}, \mathbf{q}) + \frac{1}{c^4} H_4(\mathbf{p}, \mathbf{q}), \tag{139}$$

where $H_0 = |\mathbf{p}|^2/2\mu + GM\mu/|\mathbf{q}|$ encodes the Newtonian dynamics, and $H_{2,4}$ describes pN corrections to that motion. A binary's energy and angular momentum can be found from this Hamiltonian without too much difficulty.

The next step is to write down an effective one-body metric,

$$ds^2 = -A(R)c^2 dT^2 + B(R) dR^2 + R^2(d\theta^2 + \sin^2\theta \, d\phi^2), \tag{140}$$

where $A(R) = 1 + \alpha_1(GM/Rc^2) + \alpha_2(GM/Rc^2)^2 + \ldots$; a similar expansion describes $B(R)$. The coefficients α_i depend on reduced mass ratio, $\eta = \mu/M$. The effective problem is then to describe the motion of a test body in the spacetime (Equation 140). By asserting a correspondance between certain action variables in the pN framework and in the effective framework, the coefficients α_i are completely fixed. For example, one finds that, as $\eta \to 0$, the metric (Equation 140) is simply the Schwarzschild spacetime. The effective problem can thus be regarded as the motion of a test body around a deformed black hole, with η controlling the deformation. See Damour (2008) and references therein for further discussion.

One must also describe radiation reaction in the effective one-body approach. A key innovation introduced by Damour and coworkers [see Damour, Iyer & Sathyaprakash (1998) for the original presentation of this idea] is to resume the pN results for energy loss due to GWs in order to obtain a result that is good into the strong field. In more detail, we put

$$\frac{dp_\phi}{dt} = -\mathcal{F}_\phi. \tag{141}$$

The function $\mathcal{F}_\phi$ is known to rather high order in orbital velocity v by a combination of analyses both in pN theory (see, e.g., Blanchet 2006 for a review) and to analytic expansion of results in perturbation theory (Mino et al. 1997). It can be written

$$\mathcal{F}(v) = \frac{32G}{5c^5} \eta r^4 \Omega^5 F(v), \tag{142}$$

where

$$F(v) = 1 + \sum a_n \left(\frac{v}{c}\right)^{n/2} + \sum b_n \log(v/c) \left(\frac{v}{c}\right)^{n/2}. \tag{143}$$

Post-Newtonian theory allows us to compute a_n, including contributions in μ/M, up to $n = 7$, and shows that $b_n \neq 0$ for $n = 6$ (Blanchet 2006, equation 168). Perturbation theory (Mino et al. 1997, equation 4.18) gives us the $\mathcal{O}[(\mu/M)^0]$ contributions for a_n up to $n = 11$ and shows that $b_n \neq 0$ for $n = 8, 9, 10, 11$.

The resummation introduced by Damour, Iyer & Sathyaprakash requires factoring out a pole at $v = \hat{v}$ in the function $F(v)$ and then reorganizing the remaining terms using a Padé approximant:

$$F^{\mathrm{rs}}(v) = (1 - v/\hat{v})^{-1} \, P\left[(1 - v/\hat{v})F(v)\right]. \tag{144}$$

The approximant P converts an Nth order polynomial into a ratio of $N/2$th order polynomials whose small v expansion reproduces the original polynomial:

$$P\left[1 + \sum_{n=1}^{N} c_n(v/c)^n\right] = \frac{1 + \sum_{n=1}^{N/2} d_n(v/c)^n}{1 + \sum_{n=1}^{N/2} e_n(v/c)^n}. \tag{145}$$

Using this approach to define the evolution of a system due to GW backreaction, it is not so difficult to compute the waves that a binary generates as its members spiral together. Indeed, by augmenting these waves with the ringdown that comes once the spacetime is well-described by a single black hole, the effective one-body approach has recently had great success in matching to the waveforms that are produced by numerical relativity simulations. We defer a discussion of this matching until after we have described numerical relativity in more detail, in order that the effectiveness of this comparison can be made more clear.

6. NUMERICAL RELATIVITY

Numerical relativity means the direct numerical integration of the Einstein field equations, evolving from an initial spacetime to a final state. This requires rethinking some of our ideas about GR. As a prelude, consider Maxwell's equations, written in somewhat nonstandard form:

$$\nabla \cdot \mathbf{E} = 4\pi\rho, \quad \nabla \cdot \mathbf{B} = 0; \tag{146}$$

$$\frac{\partial \mathbf{B}}{\partial t} = -c\,\nabla \times \mathbf{E}, \quad \frac{\partial \mathbf{E}}{\partial t} = 4\pi\mathbf{J} - c\,\nabla \times \mathbf{B}. \tag{147}$$

These equations tell us how $\mathbf{E}$ and $\mathbf{B}$ are related throughout spacetime. Notice that Equations 146 and 147 play very different roles here. The divergence equations contain no time derivatives; if we imagine slicing spacetime into a stack of constant time slices, then Equation 146 tells us how $\mathbf{E}$ and $\mathbf{B}$ are constrained on each slice. By constrast, the curl equations do include time operators, and so tell us how $\mathbf{E}$ and $\mathbf{B}$ are related as we evolve from slice to slice. We turn now to developing the Einstein equations into a form appropriate for evolving from an initial form; our discussion is heavily influenced by the nicely pedagogical presentation of Baumgarte & Shapiro (2003).

6.1. Overview: From Geometric Equations to Evolution Equations

How do we use Equation 29 to evolve spacetime from some initial state? The Einstein field equations normally treat space and time democratically—no explicit notion of time is built into Equation 29. The very question requires us to change our thinking: Evolving from an initial state requires some notion of time.

Suppose that we have chosen a time coordinate, defining a way to slice spacetime into space and time. We must reformulate the Einstein field equations using quantities defined solely on a given time slice. **Figure 8** illustrates how two nearby time slices may be embedded in spacetime. Once time is set, we can freely choose spatial coordinates in each slice; we show x^i on both slices.
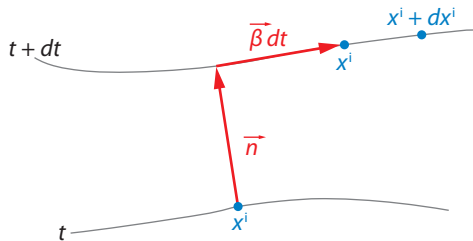
Figure 8

Slicing of spacetime into space and time. The vector $\vec{n}$ is normal to the slice at t. An observer who moves along $\vec{n}$ experiences an interval of proper time $d\tau = \alpha\, dt$, where α is the lapse function. The shift $\vec{\beta}$ describes the translation of spatial coordinates x^i from slice to slice as seen by that normal observer.

Let $\vec{n}$ be normal to the bottom slice. The lapse $\alpha \equiv d\tau/dt$ sets the proper time experienced by an observer who moves along $\vec{n}$; the shift β^i tells us by how much x^i is displaced (shifted) on the second slice relative to the normal observer. We will soon see that α and β^i are completely unconstrained by Einstein's equations. They let us set coordinates as conveniently as possible, generalizing the gauge generator ξ^μ used in linearized theory (cf. Section 3) to the strong field.

The proper spacetime separation of x^i and $x^i + dx^i$ is then

$$ds^2 = -\alpha^2 dt^2 + g_{ij}(dx^i + \beta^i dt)(dx^j + \beta^j dt). \tag{148}$$

We now have a form for the metric of spacetime, a notion of constant time slices, and the normal to a slice $\vec{n}$. Because we are interested in understanding quantities that live in a given slice (i.e., orthogonal to the normal $\vec{n}$), we build the projection tensor $\gamma_{\mu\nu} = g_{\mu\nu} + n_\mu n_\nu$. This tensor is just the metric for the geometry in each slice. We can choose coordinates so that $\gamma_{tt} = \gamma_{ti} = 0$, and $\gamma_{ij} = g_{ij}$; we will assume these from now on.

We now have enough pieces to see how to build the field equations in this formalism: We take Equation 29 and project components parallel and orthogonal to $\vec{n}$. Consider first the component that is completely parallel to $\vec{n}$:

$$G_{\alpha\beta}n^\alpha n^\beta = 8\pi G T_{\alpha\beta}n^\alpha n^\beta \rightarrow R + K^2 - K_{ij}K^{ij} = 16\pi G\rho. \tag{149}$$

(See Baumgarte & Shapiro 2003 for a detailed derivation of Equation 149.) In this equation, R is the Ricci scalar for the three-metric γ_{ij}, $\rho = T_{\alpha\beta}n^\alpha n^\beta$, and

$$\begin{aligned} K_{ij} &\equiv -\gamma_i^\alpha \gamma_j^\beta \nabla_\alpha n_\beta \\ &= \frac{1}{2\alpha}\left(-\partial_t \gamma_{ij} + D_i\beta_j + D_j\beta_i\right) \end{aligned} \tag{150}$$

is the extrinsic curvature. (The operator D_i is a covariant derivative for the metric γ_{ij}.) It describes the portion of the curvature that is due to the way that each constant time slice is embedded in the full spacetime. Equation 149 is known as the Hamiltonian constraint. (See Baumgarte & Shapiro 2003 for details of how to go from the first line of Equation 149, which is a definition, to the second line, which is more useful here.) Notice that it contains no time derivatives of K_{ij}. This equation is thus a constraint, relating data on a given timeslice.

Next, components parallel to $\vec{n}$ on one index and orthogonal on the other:

$$G_{\alpha\beta}n^\alpha \gamma_i^\beta = 8\pi G T_{\alpha\beta}n^\alpha \gamma_i^\beta \rightarrow D_j K_i^j - D_i K = 8\pi G j_i. \tag{151}$$

The matter current $j_i = -T_{\alpha\beta}n^\alpha \gamma_i^\beta$. Equation 151 is the momentum constraint; notice it also has no time derivatives of K_{ij}.

Finally, project completely orthogonal to $\vec{n}$:

$$
\begin{aligned}
G_{\alpha\beta}\gamma_i^\alpha\gamma_j^\beta = 8\pi\,G T_{\alpha\beta}\gamma_i^\alpha\gamma_j^\beta \rightarrow \\
\partial_t K_{ij} = -D_i D_j \alpha + \alpha\left[R_{ij} - 2K_{ik}K_j^k + KK_{ij} - 8\pi\,G\alpha(\text{matter})\right] \\
+ \beta^k D_k K_{ij} + K_{ik}D_j\beta^k + K_{kj}D_i\beta^k.
\end{aligned}
\tag{152}
$$

(We have abbreviated a combination of projections of the stress-energy tensor as "matter." Interested readers can find more detailed discussion in Baumgarte & Shapiro 2003.) Combining Equations 152 and 150 gives us a full set of evolution equations for the metric and the extrinsic curvature, describing how the geometry changes as we evolve from time slice to time slice.

The field equations sketched here are the ADM equations (Arnowitt, Deser & Misner 1962). Today, most groups work with modified versions of these equations; a particularly popular version is the BSSN system, developed by Baumgarte & Shapiro (1999), building on foundational work by Shibata & Nakamura (1995). In BSSN, one rewrites the spacetime metric as

$$
\tilde{\gamma}_{ij} = e^{-4\phi}\gamma_{ij},
\tag{153}
$$

where ϕ is chosen so that $e^{12\phi} = \det(\gamma_{ij})$. With this choice, $\det(\tilde{\gamma}_{ij}) = 1$. Roughly speaking, the decomposition equation (Equation 153) splits the geometry into transverse and longitudinal degrees of freedom (encapsulated by $\tilde{\gamma}_{ij}$ and ϕ, respectively). One similarly splits the extrinsic curvature into longitudinal and transverse parts by separately treating its trace and its trace-free parts:

$$
A_{ij} = K_{ij} - \frac{1}{3}\gamma_{ij}K.
\tag{154}
$$

It is convenient to conformally rescale A_{ij}, using $\tilde{A}_{ij} = e^{-4\phi}A_{ij}$. One then develops evolution equations for ϕ, $\tilde{\gamma}_{ij}$, K, and $\tilde{A}_{ij}$. See Baumgarte & Shapiro (1999) for detailed discussion.

6.2. The Struggles and the Breakthrough

Having recast the equations of GR into a form that lets us evolve forward in time, we might hope that simulating the merger of two compact bodies would now not be too difficult. In addition to the equations discussed above, we need a few additional pieces:

1. Initial data, i.e., a description of the metric and extrinsic curvature of a binary at the first moment in a simulation. Ideally, we might hope that this initial data set would be related to an earlier inspiral of widely separated bodies (e.g., Nissanke 2006, and Yunes et al. 2006). However, any method that can produce a bound binary with specified masses m_1, m_2 and spins S_1, S_2 should allow us to simulate a binary (although it may be contaminated by having the wrong GW content at early times).

2. Gauge or coordinate conditions, i.e., an algorithm by which the lapse α and shift β^i are selected. Because these functions are not determined by the Einstein field equations but are instead freely specified, they can be selected in a way that is as convenient as possible. Such wonderful freedom can also be horrible freedom, because one could choose gauge conditions that obscure the physics we wish to study, or not facilitate a stable simulation.

3. Boundary conditions. If the simulation contains black holes, then they should have an event horizon from which nothing comes out. Unfortunately, we cannot know where horizons are located until the full spacetime is built (though we have a good estimate, the apparent horizon, which can be computed from information on a single time slice). They also contain singularities. Hopefully, event horizons will prevent singular fields from contaminating the spacetime. The computation will also have an outer boundary. Far from the binary, the

spacetime should asymptote to a flat (or Robertson-Walker) form, with a gentle admixture of outgoing GWs.

How to choose these ingredients has been active research for many years. Early on, some workers were confident it was just a matter of choosing the right combination of methods and the pieces would fall into place. The initial optimism was nicely encapsulated by the following quote from Thorne (1987, p. 379):

> …numerical relativity is likely to give us, in the next five years or so, a detailed and highly reliable picture of the final coalescence and the wave forms it produces, including the dependence on the holes' masses and angular momenta.

For many years, Thorne's optimism seemed misplaced. Despite having a detailed understanding of the principles involved, it seemed simply not possible to evolve binary systems for any interesting length of time. In most cases, the binary's members could complete a fraction of an orbit and then the code would crash. As Joan Centrella has emphasized in several venues, by roughly 2004 "people were beginning to say 'numerical relativity cannot be done'" (J. Centrella, private communication).

A major issue with many of these simulations appeared to be constraint violating modes. These are solutions of the system $(\partial_t \gamma_{ij}, \partial_t K_{ij})$ that do not satisfy the constraints (Equations 149 and 151). As with the Maxwell equations, one can prove that a solution that satisfies the constraints initially will continue to satisfy them at later times in the continuum limit (cf. section IIIC of Pretorius 2007). Unfortunately, numerical relativity does not work in the continuum limit, and, even more unfortunately, constraint violating modes generically tend to be unstable (Lindblom & Scheel 2002). This means that small numerical errors can seed the modes, which then grow unstably and swamp the true solution. The challenge was to keep the seed instabilities as small as possible and then to prevent them from growing. In this way, Brügmann, Tichy & Jansen (2004) were able to compute one full orbit of a black hole binary before their simulation crashed.

It was thus something of a shock when Pretorius (2005) demonstrated a binary black hole simulation that executed a full orbit, followed by merger and ringdown to a Kerr black hole, with no crash apparent. Pretorius used a formulation of the Einstein equations based on coordinates similar to the de Donder coordinates described in Section 5. These are known as generalized harmonic coordinates; see Pretorius (2007) for detailed discussion. Because his success came with such a radically different system of equations, it was suspected that the ADM-like equations might have to be abandoned. These concerns were allayed by near simultaneous discoveries by numerical relativity groups then at the University of Texas in Browsnville (Campanelli et al. 2006) and the Goddard Space Flight Center (Baker et al. 2006). The Campanelli et al. and Baker et al. groups both used the BSSN formalism described at the end of Section 6.1. To make this approach work, they independently discovered a gauge condition that allows the black holes in their simulations to move across their computational grid. (Earlier calculations typically fixed the coordinate locations of the black holes, which means that the coordinates effectively corotated with the motion of the binary.) It was quickly shown that this approach yielded results that agreed excellently with Pretorius's setup (Baker et al. 2007).

Implementing the so-called moving puncture approach was sufficiently simple that the vast majority of numerical relativity groups were able to immediately apply it to their codes and begin evolving binary black holes. These techniques have also revolutionized our ability to model systems containing neutron stars (Shibata & Uryū 2006, Etienne et al. 2008). In the past four years, we have thus moved from a state of being barely able to model a single orbit of a compact binary system in full general relativity to being able to model nearly arbitrary binary configurations.
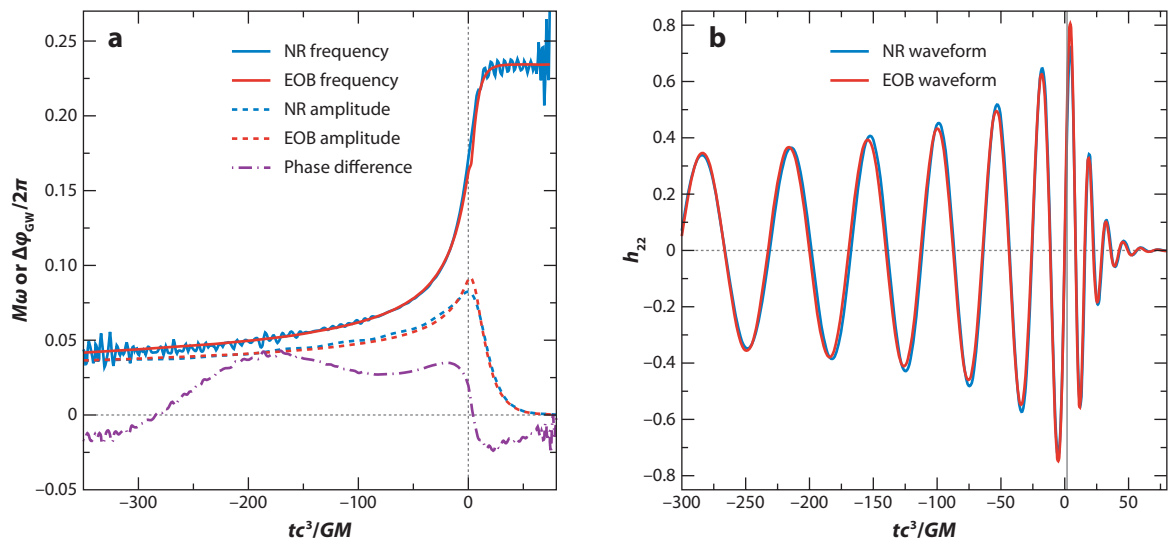
Figure 9

(*a*) Comparison between the numerical relativity (NR) computed frequency and phase and the effective one-body (EOB) frequency and phase. (*b*) Gravitational waveform computed by those two methods. These plots are for the coalescence of two nonspinning black holes with a mass ratio $m_2/m_1 = 4$. Figure kindly provided by Alessandra Buonanno; taken from Buonanno et al. (2007).

Though Thorne's 1987 prediction quoted above was far too optimistic on the timescale, his prediction for how well the physics of binary coalescence would be understood appears to be exactly correct.

6.3. Gravitational Waves from Numerical Relativity and Effective One Body

Prior to this breakthrough, the effective one-body approach gave the only strong-field description of GWs from the coalescence of two black holes. Indeed, these techniques made a rather strong prediction: The coalescence waveform should be fairly boring in the sense that we expect the frequency and amplitude to chirp up to the point at which the physical system is well modeled as a single deformed black hole. Then, it should rapidly ring down to a quiescent Kerr state.

Such a waveform is indeed exactly what numerical simulations exhibit. It has since been found that predictions from the effective one-body formalism give an outstanding description of the results from numerical relativity. There is some freedom to adjust how one matches effective one-body waves to the numerical relativity output (e.g., the choice of pole $\hat{v}$ in Equation 144); Buonanno et al. (2007) and Damour et al. (2008) describe how to do this matching.

Figure 9, taken from Buonanno et al. (2007), gives an example of how well the waveforms match one another. Over the entire span computed, the two waveforms differ in phase by only a few hundredths of a cycle. The agreement is so good that one can realistically imagine calibrating the effective one-body waveforms with a relatively small number of expensive numerical relativity computations, and then densely sampling the binary parameter space using the effective one-body approach.

7. GRAVITATIONAL-WAVE RECOIL

That GWs carry energy and angular momentum from a binary, driving its members to spiral together as described in Section 3.3, is widely appreciated. Until recently, it was not so well

appreciated that the waves can carry linear momentum as well. If the binary and its radiation pattern are asymmetric, then that radiation carries a net flux of momentum given by

$$\frac{dp^i}{dt} = R^2 \int d\Omega \, T^{00} n^i, \tag{155}$$

where T^{00} is the energy-flux component of the Isaacson tensor (Equation 71), n^i is the ith component of the radial unit vector, and the integral is taken over a large sphere ($R \to \infty$) around the source. Recent work has shown that the contribution to this kick from the final plunge and merger of coalescing black holes can be particularly strong. We now summarize the basic physics of this effect and survey recent results.

Bekenstein (1973) appears to have first appreciated that the momentum flux of GWs could have interesting astrophysical consequences. Fitchett (1983) then estimated the impact this flux could have on a binary. An aspect of the problem that Fitchett's analysis makes very clear is that the recoil comes from the beating of different multipolar contributions to the recoil: If one only looks at the quadrupole part of the GWs (cf. Equation 53), the momentum flux is zero. Fitchett's analysis included octupole and current-quadrupole radiation, and he found

$$v_{\text{kick}} \simeq 1450 \, \text{km/sec} \frac{f(q)}{f_{\text{max}}} \left(\frac{GM_{\text{tot}}/c^2}{R_{\text{term}}} \right)^4, \tag{156}$$

where $f(q) = q^2(1-q)/(1+q)^5$ gives the dependence on mass ratio $q = m_1/m_2$. This function has a maximum at $q \simeq 0.38$. The radius R_{term} describes when wave emission cuts off; for systems containing black holes this scales with the total mass. Thus, the recoil does not depend on total mass, just mass ratio.

Fitchett's analysis is similar to our discussion in Section 3.3 in that Newtonian dynamics are supplemented with multipolar wave emission. Because the effect is strongest when R_{term} is smallest, it was long clear that a proper relativistic analysis was needed to get this kick correct. [Indeed, a prescient analysis by Redmount & Rees (1989) suggested that binaries containing rapidly spinning black holes were likely to be especially interesting; as we shall see below, they were absolutely correct.]

Favata, Hughes & Holz (2004) provided the first estimates of recoil where the strong-field physics are done more or less correctly. They used the perturbative techniques described in Section 4, arguing that one can extrapolate from the small mass ratio regime to $q \sim 0.2$ or so with errors of a few tens of percent. Unfortunately, their code at that time did not work well with plunging orbits, so they had large error bars. They did find, however, that the maximum recoil probably fell around $v_{\text{kick}} \simeq (250 \pm 150) \, \text{km sec}^{-1}$, at least if no more than one body spins, and if the spin and orbit are aligned. Blanchet, Qusailah & Will (2005) revisited this treatment, with a particular eye on the final plunge waves, using the pN methods outlined in Section 5. Their results were consistent with those of Favata et al., but reduced the uncertainty substantially, finding $v_{\text{kick}} \simeq (220 \pm 50) \, \text{km sec}^{-1}$.

These numbers stood as the state of the art in black hole recoil for several years, until numerical relativity's breakthrough (Section 6) made it possible to study black hole mergers without any approximations. The Favata et al. and Blanchet et al. numbers turn out to agree quite well with predictions for the merger of nonspinning black holes; González et al. (2007) find the maximum kick for nonspinning merger comes when $q = 0.38$, yielding $v_{\text{kick}} = (175 \pm 11) \, \text{km sec}^{-1}$. When spin is unimportant, kicks appear to be no larger than a few hundred kilometers per second.

When spin is important, the kick can be substantially larger. Recent work by Campanelli et al. (2007) shows that when the holes have large spins (near the Kerr maximum $a = M$), and those spins are aligned just right (equal in magnitude, antiparallel to each other, and orthogonal to the

orbital angular momentum), the recoil can be a few thousand kilometers per second. Exploration of binary black hole parameter space is needed to assess how much of this maximum is actually achieved; early work on this problem is finding that large kicks (many hundreds to a few thousands of kilometers per second) can be achieved for various spin orientations as long as the spins are large (Tichy & Marronetti 2007, Pollney et al. 2007). That the maximum is so much higher than had been appreciated suggests that substantial recoils may be more common than the Favata et al. and Blanchet et al. calculations led us to expect (Schnittman & Buonanno 2007).

Many recent papers have emphasized that kicks could have strong astrophysical implications, ranging from escape of the black hole from its host galaxy to shocks in material accreting onto the large black hole. The first possible detection of black hole recoil was recently announced (Komossa, Zhou & Lu 2008). As that claim is assessed, we anticipate much activity as groups continue to try to identify a signature of a recoiling black hole.

8. ASTRONOMY WITH GRAVITATIONAL WAVES

Direct GW measurement is a major motivator for theorists seeking to understand how binary systems generate these waves. In this section, we first summarize the principles behind modern interferometric GW detectors. Given that these principles are likely to be novel for much of the astronomical community, we present this material in some depth. Note that Finn (2008) has recently flagged some important issues in the standard calculation of an interferometer's response to GWs (which, however, do not change the final results). For the sake of brevity, we omit these issues and recommend his article for those wishing a deeper analysis. We then briefly describe existing and planned detectors, and describe how one measures a binary's signal with these instruments. This last point highlights why theoretical modeling has been so strongly motivated by the development of these instruments.

8.1. Principles Behind Interferometric GW Antennae

As a simple limit, treat the spacetime in which our detector lives as flat plus a simple GW propagating down our coordinate system's z-axis:

$$ds^2 = -dt^2 + (1+h)dx^2 + (1-h)dy^2 + dz^2, \tag{157}$$

where $h = h(t - z)$. We neglect the influence of the Earth (clearly important for terrestrial experiments) and the solar system (which dominates the spacetime of space-based detectors). Corrections describing these influences can easily be added to Equation 157; we neglect them because they represent influences that vary on much longer timescales than those of the GWs.

Figure 10 sketches an interferometer that can measure a GW. Begin by examining the geodesics describing the masses at the ends of the arms and the beam splitter at the center. Take these objects to be initially at rest, so that $(dx^\mu/d\tau)_{\text{before}} \doteq (1, 0, 0, 0)$. The GW shifts this velocity by an amount of order the wave strain: $(dx^\mu/d\tau)_{\text{after}} = (dx^\mu/d\tau)_{\text{before}} + \mathcal{O}(h)$. Now examine the geodesic equation

$$\frac{d^2x^j}{d\tau^2} + \Gamma^j_{\alpha\beta}\frac{dx^\alpha}{d\tau}\frac{dx^\beta}{d\tau} = 0. \tag{158}$$

All components of the connection are $\mathcal{O}(h)$. Combining this with our argument for how the GW affects the various velocities, we have

$$\frac{d^2x^j}{d\tau^2} + \Gamma^j_{00}\frac{dx^0}{d\tau}\frac{dx^0}{d\tau} + \mathcal{O}(h^2) = 0. \tag{159}$$
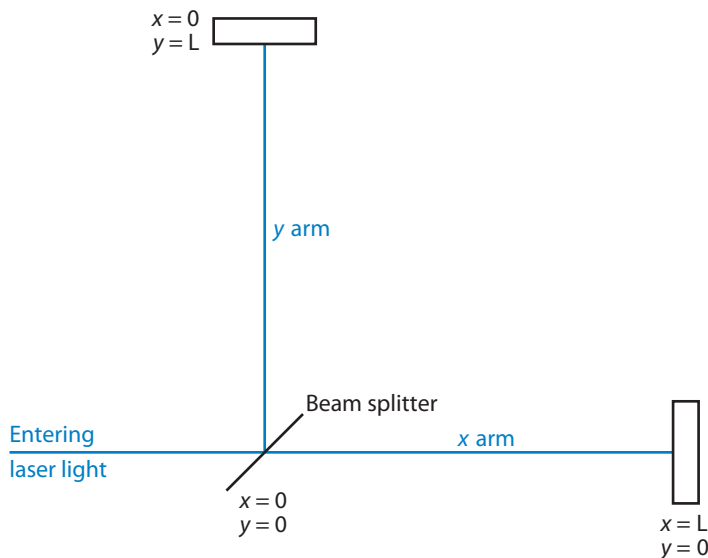
Figure 10

Schematic of an interferometer that could be used to detect GWs. Though real interferometers are vastly
more complicated, this interferometer topology contains enough detail to illustrate the principle by which
such measurements are made.

Now,

$$\Gamma^j_{00} = \frac{1}{2} g^{jk} \left(\partial_0 g_{k0} + \partial_0 g_{0k} - \partial_k g_{00} \right) = 0. \tag{160}$$

Thus,

$$\frac{d^2 x^j}{d\tau^2} = 0. \tag{161}$$

The test masses are unaccelerated to leading order in the GW amplitude h.

This seems to say that the GW has no impact on the masses. However, the geodesic equation
describes motion with respect to a specified coordinate system. These coordinates are effectively
comoving with the interferometer's components. This is convenient because the interferometer's
components remain fixed in our coordinates. Using this, we can show that the proper length of
the arms does change. For instance, the x-arm has a proper length

$$D_x = \int_0^L \sqrt{g_{xx}} \, dx = \int_0^L \sqrt{1 + h} \, dx \simeq \int_0^L \left(1 + \frac{h}{2} \right) dx = L \left(1 + \frac{h}{2} \right). \tag{162}$$

Likewise, the y-arm has a proper length $D_y = L(1 - h/2)$.

The armlengths as measured by a ruler will vary with h. One might worry, though, that the
ruler will vary, cancelling the measurement. This does not happen because rulers are not made
of freely falling particles: The elements of the ruler are bound to one another and act against the
GW. The ruler will feel some effect from the GW, but it will be far smaller than the variation in
the separation.

The ruler used by the most sensitive current and planned detectors is based on laser inter-
ferometry. We now briefly outline how a GW imprints itself on the phase of the interferometer
sketched in **Figure 10**. For further discussion, we recommend Faraoni (2007); we also recommend
Finn (2008) for more detailed discussion. In the interferometer shown, laser light enters from the
left, hits the beam splitter, travels down both the x and y arms, bounces back, and is recombined

at the beam splitter. Begin with light in the x arm and compute the phase difference between light that has completed a round trip and light that is just entering. The phase of a wavefront is constant as it follows a ray through spacetime, so we write this difference as

$$\Delta\Phi_x \equiv \Phi(T_{\text{round-trip}}) - \Phi(0) = \omega_{\text{proper}} \times (\text{proper round-trip travel time}), \tag{163}$$

where ω_{proper} is the laser frequency measured by an observer at the beam splitter. Detecting a GW is essentially precision timing, with the laser acting as our clock.

Consider first the proper frequency. Light energy as measured by some observer is $E = -\vec{p} \cdot \vec{u}$, where $\vec{p}$ is the light's four-momentum and $\vec{u}$ is the observer's four-velocity. We take this observer to be at rest, so

$$E = -p_t = -g_{tt}p^t = p^t. \tag{164}$$

Put $p^\mu = \hat{p}^\mu + \delta p^\mu$, where $\hat{p}^\mu$ describes the light in the absence of a GW, and δp^μ is a GW shift. In the x arm, $\hat{p}^\mu \doteq \hbar\omega(1, \pm1, 0, 0)$; the signs correspond to before and after the bounce. We compute the shift δp^μ using the geodesic equation (Equation 12):

$$\frac{d\delta p^\mu}{d\chi} + \Gamma^\mu_{\alpha\beta}\hat{p}^\alpha\hat{p}^\beta = 0. \tag{165}$$

(We use $d\hat{p}^\mu/d\chi = 0$ in the background to simplify.) Focus on the $\mu = t$ component. The only nontrivial connection is $\Gamma^t_{xx} = \partial_t h/2$. Using in addition the facts that $p^\mu = dx^\mu/d\chi$ plus $\hat{p}^t = \pm\hat{p}^x$ reduces the geodesic equation to

$$\frac{d\delta p^t}{dt} = -\frac{1}{2}\hat{p}^t\partial_t h. \tag{166}$$

Integrating over a round trip, we find

$$\delta p^t = -\frac{\hat{p}^t}{2}\left[h(T_{\text{round-trip}}) - h(0)\right]. \tag{167}$$

So, we finally find the proper frequency:

$$\begin{aligned}\omega_{\text{proper}} &\equiv E/\hbar = \omega\left\{1 + \tfrac{1}{2}\left[h(0) - h(T_{\text{round-trip}})\right]\right\}\\ &\simeq \omega.\end{aligned} \tag{168}$$

On the second line of Equation 168, we take $T_{\text{round-trip}}$ to be much smaller than the wave period. This is an excellent approximation for ground-based interferometers; the exact result must be used for high-frequency response in space.

Turn next to the proper round-trip time. The metric (Equation 157) shows us that proper time measured at fixed coordinate is identical to the coordinate time t. For light traveling in the x arm, $0 = -c^2dt^2 + (1 + h)dx^2$, so

$$dx = \pm c\,dt\left(1 - \frac{h}{2}\right) + \mathcal{O}(h^2). \tag{169}$$

Now integrate over x from 0 to L and back, and over t from 0 to $T_{\text{round-trip}}$:

$$\begin{aligned}2L &= c\,T_{\text{round-trip}} - \frac{c}{2}\int_0^{T_{\text{round-trip}}} h\,dt\\ &= c\,T_{\text{round-trip}} - \frac{c}{2}\int_0^{2L/c} h\,dt + \mathcal{O}(h^2).\end{aligned} \tag{170}$$

We thus find

$$T_{\text{round-trip}} = \frac{2L}{c} + \frac{1}{2}\int_0^{2L/c} h\, dt$$
$$\simeq \frac{2L}{c}\left(1 + \frac{1}{2}h\right). \tag{171}$$

The second line describes a wave that barely changes during a round trip.

The total phase change is found by combining Equations 163, 168 and 171:

$$\Delta\Phi_x = \omega\left(\frac{2L}{c} + \frac{1}{2}\int_0^{2L/c} h\, dt\right)\left(1 + \tfrac{1}{2}\left[h(0) - h(2L/c)\right]\right)$$
$$\simeq \frac{2\omega L}{c}\left(1 + \frac{1}{2}h\right). \tag{172}$$

The second line is for a slowly varying wave, and the first is exact to order h. We use the slow limit in further calculations. Repeating for the y arm yields

$$\Delta\Phi_y = \frac{2\omega L}{c}\left(1 - \frac{1}{2}h\right). \tag{173}$$

Notice that this GW acts antisymmetrically on the arms. By contrast, any laser phase noise will be symmetric: Because the same laser state is sent into the arms by the beam splitter, we have $\Delta\Phi_x^{\text{Noise}} = \Phi_y^{\text{Noise}}$. We take advantage of this by reading out light produced by destructive interference at the beam splitter:

$$\Delta\Phi^{\text{Read-out}} = \Delta\Phi_x - \Delta\Phi_y = \left(\Delta\Phi_x^{\text{GW}} + \Delta\Phi_x^{\text{Noise}}\right) - \left(\Delta\Phi_y^{\text{GW}} + \Delta\Phi_y^{\text{Noise}}\right)$$
$$= 2\Delta\Phi_x^{\text{GW}}. \tag{174}$$

An L-shaped interferometer is sensitive only to the GW, not to laser phase noise. This is the major reason that this geometry is used; even if an incident wave is oriented such that the response of the arms to the GW is not asymmetric, one is guaranteed that phase noise will be cancelled by this configuration.

From basic principles we turn now to a brief discussion of current and planned detectors. Our goal is not an in-depth discussion, so we refer readers interested in these details to excellent reviews by Hough & Rowan (2000) (which covers in detail the characteristics of the various detectors) and Tinto & Dhurandar (2005) (which covers the interferometry used for space-based detectors).

8.2. Existing and Planned Detectors

When thinking about GW detectors, a key characteristic is that the frequency of peak sensitivity scales inversely with armlength. The ground-based detectors currently in operation (and undergoing or about to undergo upgrades) are sensitive to waves oscillating at 10s–1000s of Hertz. Planned space-based detectors will have sensitivities at much lower frequencies, ranging from 10^{-4}–0.1 Hz (corresponding to waves with periods of tens of seconds to hours).

The ground-based detectors currently in operation are LIGO (Laser Interferometer Gravitational-Wave Observatory), with antennae in Hanford, Washington and Livingston, Louisiana; Virgo near Pisa, Italy; and GEO near Hanover, Germany. The LIGO interferometers each feature 4-km arms and have a peak sensitivity near 100 Hz. Virgo is similar, with 3-km arms and sensitivity comparable to that of the LIGO detectors. GEO (or GEO600) has 600-m arms; as such, its peak sensitivity is at higher frequencies than LIGO and Virgo. By using advanced interferometry techniques, it is able to achieve sensitivity competitive with the kilometer-scale instruments. All of these instruments will be upgraded over the course of the next few years,

installing more powerful lasers and reducing the impact of local ground vibrations. The senstivity of LIGO should be improved by roughly a factor of ten, and the bandwidth should be increased as well. See Fritschel (2003) for detailed discussion.

There are also plans to build additional kilometer-scale instruments. The detector AIGO (Australian International Gravitational Observatory) is planned as a detector very similar to LIGO and Virgo, but in Western Australia (McClelland 2002). This location, far from the other major GW observatories, has great potential to improve the ability of the worldwide GW detector network to determine the characteristics of GW events (Searle et al. 2006). In particular, AIGO should be able to break degeneracies in angles that determine a source's sky position and polarization, greatly adding to the astronomical value of GW observations. The Japanese GW community, building on their experience with the 300-m TAMA interferometer, hopes to build a 3-km underground instrument. Dubbed LCGT (Large-Scale Cryogenic Gravitational Wave Telescope), the underground location will take advantage of the fact that local ground motions tend to decay fairly rapidly as we move away from the Earth's surface. They plan to use cryogenic cooling to reduce noise from thermal vibrations.

In space, the major project is LISA (*Laser Interferometer Space Antenna*), a 5-million-kilometer interferometer under development as a joint NASA-ESA mission. LISA will consist of three spacecraft placed in orbits such that their relative positions form an equilateral triangle whose centroid lags the Earth by 20° and whose plane is inclined to the ecliptic by 60°; see **Figure 11**. Because the spacecraft are free, they do not maintain this constellation precisely; however, the variations in armlength occur on a timescale far longer than the periods of their target waves, and so can be modeled out without too much difficulty. The review by Tinto & Dhurandar (2005) discusses in great detail how one does interferometry on such a baseline with time-changing armlengths. LISA is being designed to target waves with periods of several hours to several seconds, a particularly rich band for signals involving black holes that have $10^5 \, M_\odot \lesssim M \lesssim 10^7 \, M_\odot$.

Somewhat smaller than LISA, The Japanese GW community has proposed DECIGO (*DECI-hertz Interferometer Gravitational Wave Observatory*), a space antenna to target a band at roughly 0.1 Hz. This straddles the peak sensitivities of LISA and terrestrial detectors and may thus act as a
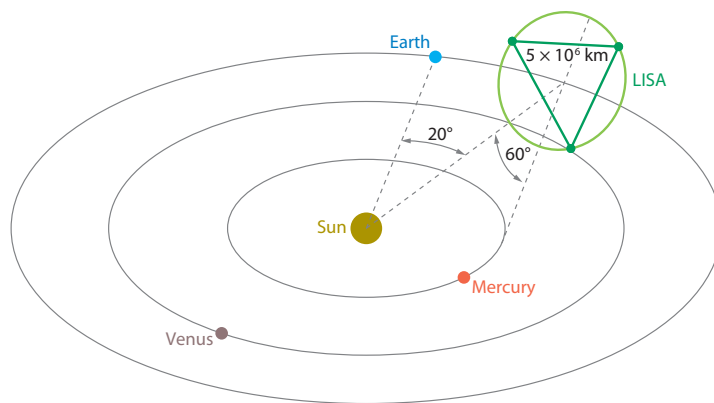
Figure 11

Schematic of the LISA constellation in orbit about the Sun. Each arm of the triangle is 5×10^6 km; the centroid of the constellation lags the Earth by 20°, and its plane is inclined to the ecliptic by 60°. Note that the spacecraft orbit freely; there is no formation flying in the LISA configuration. Instead, each spacecraft is in a slightly eccentric, slightly inclined orbit; their individual motions preserve the near-equilateral triangle pattern with high accuracy for a timescale of decades.

bridge for signals that evolve from one band to the other. See Kawamura et al. (2006) for further discussion. It is worth noting that, in addition to these laser interferometers, there have been proposals to measure gravitational waves using atom interferometry. A particularly interesting proposal has been developed by Dimopolous et al. (2008). Sources of noise in such experiments are quite different than in the case of laser interferometers, and they may usefully complement the existing suite of detectors in future applications.

8.3. Measuring Binary Signals

The central principle guiding the measurement of GWs is that their weakness requires phase coherent signal measurement. This is similar to how one searches for a pulsar in radio or X-ray data. For pulsars, one models the signal as a sinusoid with a phenomenological model for frequency evolution:

$$\Phi(t; \Phi_0, f_0, \dot{f}_0, \ddot{f}_0, \ldots) = \Phi_0 + 2\pi \left(f_0 t + \frac{1}{2}\dot{f}_0 t^2 + \frac{1}{6}\ddot{f}_0 t^3 + \cdots \right). \tag{175}$$

The cross correlation of a model, $\cos[\Phi]$, with data is maximized when the parameters $(\Phi_0, f_0, \dot{f}_0, \ddot{f}_0, \ldots)$ accurately describe a signal's phase. For a signal that is N cycles long, it is not too difficult to show that the cross correlation is enhanced by roughly $\sqrt{N}$ when the template matches the data.

For binary GWs, one similarly cross correlates models against data, looking for the template that maximizes the correlation. Imagine, for example, that the rule given by Equation 88 accurately described binary orbits over the band of our detectors. We would then expect a model based on

$$\Phi(t; \Phi_c, t_c, \mathcal{M}) = \Phi_c - \left[\frac{c^3(t_c - t)}{5G\mathcal{M}} \right]^{5/8} \tag{176}$$

to give a large correlation when the coalescence phase Φ_c, coalescence time t_c, and chirp mass $\mathcal{M}\mathcal{M}$ are chosen well. As we have discussed at length, Equation 88 is not a good model for strong-field binaries. The need to faithfully track what nature throws at us has been a major motivation for the developments in perturbation theory, pN theory, and numerical relativity discussed here.

When one determines that some set of parameters maximizes the correlation, that set is an estimator for the parameters of the binary. More formally, the cross correlation defines a likelihood function, which gives the probability of measuring some set of parameters from the data (Finn 1992). By examining how sharply the likelihood falls from this maximum, one can estimate how accurately data determines parameters. For large cross correlation (large signal-to-noise ratio), this is simply related to how the wave models vary with parameters. Let θ^a represent the ath parameter describing a waveform h. If $\langle h|h \rangle$ denotes the cross correlation of h with itself, then define the covariance matrix

$$\Sigma^{ab} = \left(\left\langle \frac{\partial h}{\partial \theta^a} \,\middle|\, \frac{\partial h}{\partial \theta^b} \right\rangle \right)^{-1} \tag{177}$$

(where the -1 power denotes matrix inverse). Diagonal elements of this matrix are $1 - \sigma$ parameter errors; off-diagonal elements describe parameter correlations. See Finn (1992) for derivations and much more detailed discussion. In the discussion that follows, we use Equation 177 to drive the discussion of how model waveforms are used to understand how well observations will be able to determine the properties of GW-generating systems.

8.4. What We Learn by Measuring Binary Gravitational Waves

8.4.1. Overview. Given all that we have discussed, what can we learn by observing compact binary merger in GWs? To set the context, consider again the Newtonian waveform

$$h_+ = -\frac{2G\mathcal{M}}{c^2 D}\left(\frac{\pi G\mathcal{M}f}{c^3}\right)^{2/3}(1 + \cos^2\iota)\cos 2\Phi_N(t),$$

$$h_\times = -\frac{4G\mathcal{M}}{c^2 D}\left(\frac{\pi G\mathcal{M}f}{c^3}\right)^{2/3}\cos\iota\,\sin 2\Phi_N(t); \qquad (178)$$

$$\Phi_N(t) = \Phi_c - \left[\frac{c^3(t_c - t)}{5G\mathcal{M}}\right]^{5/8}.$$

A given interferometer measures a combination of these two polarizations, with the weights set by the interferometer's antenna response functions:

$$h_{\text{meas}} = F_+(\theta, \phi, \psi)h_+ + F_\times(\theta, \phi, \psi)h_\times. \qquad (179)$$

The angles (θ, ϕ) give a sources position on the sky; the angle ψ (in combination with ι) describes the orientation of the binary's orbital plane with respect to a detector. See Thorne (1987, their equations 103 and 104) for further discussion.

Imagine that Equation 178 accurately described GWs in nature. By matching the phase with the data, measurement of the GW would determine the chirp mass $\mathcal{M}$. Calculations using Equation 177 to estimate measurement error (Finn & Chernoff 1993) show that $\mathcal{M}$ should be determined with exquisite accuracy, $\Delta\mathcal{M}/\mathcal{M} \propto 1/N_{\text{cyc}}$, where N_{cyc} is the number of GW cycles measured in our band.

The amplitude of the signal is determined with an accuracy $\Delta\mathcal{A}/\mathcal{A} \sim 1/\text{SNR}$. This means that, for a given GW antenna, a combination of the angles $\theta, \phi, \iota, \psi$, and the source distance D are measured with this precision; however, those parameters are not invidually determined. A single interferometer cannot break the distance-angle correlations apparent in Equations 178 and 179. Multiple detectors (which will each have its own response functions F_+ and $F_\times$) are needed to measure these source characteristics. This is one reason that multiple detectors around the globe are being built. (For LISA, the constellation's motion around the Sun makes F_+ and $F_\times$ effectively time varying. The modulation imposed by this time variation means that the single LISA antenna can break these degeneracies, provided that a source is sufficiently long lived for the antenna to complete a large fraction of an orbit.)

As we have discussed, Equation 178 does not give a good description of GWs from strong-field binaries. Effects that this Newtonian-gravity-plus-quadrupole-waves treatment misses come into play. Consider the pN phase function of Equation 132. Not only does the chirp mass $\mathcal{M}$ influence the phase, so too does the binary's reduced mass μ and its spin-orbit and spin-spin parameters β and σ. The pN phasing thus encodes more detail about the binary's characteristics. Unfortunately, these parameters may be highly correlated. For example, Cutler & Flanagan (1994) show that when precession is neglected, errors in a binary's reduced mass and spin-orbit parameter are typically 99% or more correlated with each other. This is because the time dependence of their contributions to the phase is not very different.

These correlations can be broken when we make our models more complete. As we have discussed, the spin precession equations (Equations 122 and 123) cause β and σ to oscillate. This modulates the waves' phase; as first demonstrated by Vecchio (2004) and then examined in greater depth by Lang & Hughes (2006), the modulations break parameter degeneracies and improve our ability to characterize the system whose waves we measure. **Figure 12**, taken from Lang & Hughes (2006), shows this effect for LISA measurements of coalescing binary black holes. Accounting for precession improves the accuracy with which the reduced mass is measured by roughly two
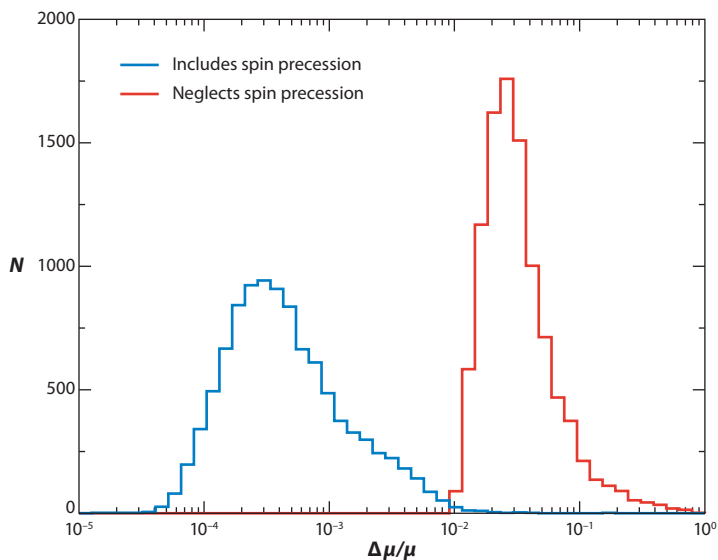
Figure 12

Accuracy with which reduced mass μ is measured by LISA for binaries at $z = 1$ with masses $m_1 = 3 \times 10^5 \, M_\odot$ and $m_2 = 10^6 \, M_\odot$. The two curves come from a Monte-Carlo simulation in which the sky is populated with 10^4 binaries whose positions, orientations, and spins have been randomly chosen. Horizontal axis is the logarithmic error $\Delta\mu/\mu$; vertical axis is the number of binaries that fall in an error bin. The dashed line neglects spin precession effects; note that the distribution peaks at an error bin of $\Delta\mu/\mu \simeq 0.03$. The solid line includes spin precession; note that the peak error is smaller by roughly two orders of magnitude.

orders of magnitude. We similarly find that the members' spins can be determined with excellent accuracy. GW measurements will be able to map the mass and spin distributions of coalescing binaries.

Equation 178 is also deficient in that only the leading quadrupole harmonic is included. As the discussion in Section 5.2.1 indicates, that is just one harmonic among many that contribute to the binary's GWs. Recent work (Arun et al. 2007, Porter & Cornish 2008, Trias & Sintes 2008) has looked at how our ability to characterize a source improves when those higher harmonics are included. Typically, one finds that these harmonics improve our ability to determine a binary's orientation ι. This is largely because each harmonic has a slightly different functional dependence on ι, so each encodes that information somewhat differently than the others. The unique functional dependence of each harmonic on ι in turn helps break degeneracies between that angle and the source distance D.

8.4.2. Bothrodesy: mapping black hole spacetimes. Extreme mass ratio captures may allow a unique GW measurement: We may use them to map the spacetimes of large black holes and test how well they satisfy the (rather stringent) requirements of GR. As discussed in Section 4, an extreme mass ratio inspiral is essentially a sequence of orbits. Thanks to the mass ratio, the small body moves through this sequence slowly, spending a lot of time close to any orbit in the sequence. Also thanks to the mass ratio, each orbit's properties are mostly determined by the larger body. In analogy to geodesy, the mapping of Earth's gravity with satellite orbits, one can imagine bothrodesy, the mapping of a black hole's gravity by studying the orbits of inspiraling satellites. (The name bothrodesy was coined by Sterl Phinney and comes from the word $\beta o\theta\rho o\varsigma$, which refers to a sacrificial pit in ancient Greek.)

In more detail, consider first Newtonian gravity. The exterior potential of a body of radius R can be expanded in a set of multipole moments:

$$\Phi_N = -\frac{GM}{r} + G \sum_{l=2}^{\infty} \left(\frac{R}{r}\right)^{l+1} M_{lm} Y_{lm}(\theta, \phi). \qquad (180)$$

Studying orbits allows us to map the potential Φ_N, and thus to infer the moments M_{lm}. By enforcing Poisson's equation in the interior, $\nabla^2 \Phi_N = 4\pi G\rho$, and then matching at the surface R, one can relate the moments M_{lm} to the distribution of matter. In this way, orbits allow us to map in detail the distribution of matter in a body like the Earth.

Bothrodesy applies the same basic idea to a black hole. The spacetime of any stationary, axisymmetric body can be described by a set of mass moments M_l, similar to the M_{lm} of Equation 180, and a set of current moments S_l, which describe the distribution of mass-energy's flow. What makes this test powerful is that the moments of a black hole take a simple form: for a Kerr black hole (Equation 99) with mass M and spin parameter a,

$$M_l + i S_l = M(ia)^l. \qquad (181)$$

A black hole has a mass moment $M_0 = M$ and a current moment $S_1 = aM$ (i.e., the magnitude of its spin is aM, modulo factors of G and c). Once those moments are known, all other moments are fixed if the Kerr solution describes the spacetime. This is a restatement of the no-hair theorem (Carter 1971, Robinson 1975), that a black hole's properties are set by its mass and spin.

The fact that an object's spacetime (and hence orbits in that spacetime) is determined by its multipoles, and that the Kerr moments take such a simple form, suggests a simple consistency test: Develop an algorithm for mapping a large object's moments by studying orbits of that object, and check that the $l \geq 2$ moments satisfy Equation 181. Ryan (1995) first demonstrated that such a measurement can in principle be done, and Brink (2008) has recently clarified what must be done for such measurements to be done in practice. Collins & Hughes (2004) took the first steps in formulating this question as a null experiment (with the Schwarzschild solution as the null hypothesis). Glampedakis & Babak (2006) formulated a similar approach appropriate to Kerr black holes, and Vigeland (S. Vigeland & S. Hughes, in preparation) has recently extended the Collins & Hughes formalism in that direction.

A robust test of the Kerr solution is thus a very likely outcome of measuring waves from extreme mass ratio captures. If, however, testing metrics is not your cup of tea, precision black hole metrology may be: In the process of mapping a spacetime, one measures with exquisite accuracy both the mass and the spin of the large black hole. Barack & Cutler (2004) have found that in most cases these events allow us to determine both the mass and the spin of the large black hole with 0.1% errors or better.

8.4.3. Binary inspiral as a standard siren. A particularly exciting astronomical application of binary inspiral comes from the fact that the GWs depend on, and thus directly encode, distance to a source. Binary inspiral thus acts as a standard candle (or standard siren, so named because it is often useful to regard GWs as soundlike), with GR providing the standardization. Schutz (1986) first demonstrated the power of GW observations of merging binaries to pin down the Hubble constant; Finn & Chernoff (1993) analyzed Schutz's argument in more detail, in addition assessing how well other cosmological parameters could be determined. More recently, Holz & Hughes (2005) have examined what can be done if a GW merger is accompanied by an electromagnetic counterpart of some kind. We now describe how inspiral waves can serve as a standard siren.

Imagine that we measure a nearby source, so that cosmological redshift can be neglected. The measured waveform generically has a form

$$h = \frac{GM(m_i)}{c^2 r} \mathcal{A}(t) \cos \left[\Phi(t; m_i, \mathbf{S}_i) \right],$$

(182)

where m_i are the binary's masses, $\mathbf{S}_i$ are its spins, and $M(m_i)$ is a function of the masses with dimension mass. For example, for the Newtonian quadrupole waveform (Equation 87), this function is the chirp mass, $M(m_i) = \mathcal{M} = (m_1 m_2)^{3/5}/(m_1 + m_2)^{1/5}$. The function $\mathcal{A}(t)$ is a slowly varying, dimensionless function that depends most strongly on parameters such as the source inclination ι.

Now place this source at a cosmological distance. Careful analysis shows that the naive Euclidean distance measure r should be the proper motion distance D_M (Carroll 2004, Chapter 8); see, e.g., Finn & Chernoff (1993) for a derivation. Also, all timescales that characterize the source will be redshifted: If τ is a timescale characterizing the source's internal dynamics, $\tau \to (1 + z)\tau$.

What is the phase Φ for this cosmological binary? Because it evolves solely due to gravity, any parameter describing the binary's dynamics enters as a timescale. For example, a mass parameter becomes a time: $m \to \tau_m \equiv Gm/c^3$. This time suffers cosmological redshift; the mass that we infer by measuring it is likewise redshifted: $m_{\text{meas}} = (1 + z)m_{\text{local}}$. Spin variables pick up a squared redshift factor: $S_{\text{meas}} = (1 + z)^2 S_{\text{local}}$. This tells us that redshift ends up degenerate with other parameters: A binary with masses m_i and spins $\mathbf{S}_i$ at redshift z has a phase evolution that looks just like a binary with $(1 + z)m_i$, $(1 + z)^2 \mathbf{S}_i$ in the local universe. So, if we put our source at redshift z, Equation 182 becomes

$$h = \frac{GM(m_i)}{c^2 D_M} \mathcal{A}(t) \cos \left[\Phi(t; (1 + z)m_i, (1 + z)^2 \mathbf{S}_i) \right].$$

(183)

Recall that proper motion distance is related to luminosity distance by $D_m = D_L/(1 + z)$. Because we do not measure masses but rather $(1 + z)$ times masses, it makes sense to adjust the amplitude and put

$$h = \frac{G(1 + z)M(m_i)}{c^2 D_L} \mathcal{A}(t) \cos \left[\Phi(t; (1 + z)m_i, (1 + z)^2 S_i) \right].$$

(184)

The key point here is that measurements directly encode the luminosity distance to a source, D_L; however, they do not tell us anything about a source's redshift z. In this sense GW measurements of merging binaries can be distance probes that are highly complementary to most other astronomical distance measures. Indeed, analyses indicate that the distance should be measured to $\sim$10–20% accuracy using ground-based instruments (e.g., Cutler & Flanagan 1994) and to $\sim$1–5% from space (Lang & Hughes 2006, Arun et al. 2007, Porter & Cornish 2008, Trias & Sintes 2008).

Suppose that we measure GWs from a merging compact binary, allowing us to measure D_L with this accuracy. If it is possible to measure the source's redshift [either from the statistical properties of the distribution of events, as emphasized by Schutz (1986) and Chernoff & Finn (1993), or by direct association with an electromagnetic event (Holz & Hughes 2005)], then one may be able to accurately determine both distance and redshift for that event—a potentially powerful constraint on the universe's cosmography with completely different systematic properties than other standard candles.

DISCLOSURE STATEMENT

The author is not aware of any affiliations, memberships, funding, or financial holdings that might be perceived as affecting the objectivity of this review.

ACKNOWLEDGMENTS

LITERATURE CITED

Armitage PJ, Natarajan P. 2002. *Ap. J. Lett.* 567:L9–12

Arnowitt R, Deser S, Misner CW. 1962. In *Gravitation: An Introduction to Current Research*, ed. L Witten, p. 227. New York: Wiley

Arun KG, Iyer BR, Sathyaprakash BS, Sinha S, van den Broeck C. 2007. *Phys. Rev. D* 76(10):104016

Baker JG, Campanelli M, Pretorius F, Zlochower Y. 2007. *Class. Quantum Gravity* 24:25

Baker JG, Centrella J, Choi D-I, Koppitz M, van Meter J. 2006. *Phys. Rev. Lett.* 96(11):111102

Barack L, Cutler C. 2004. *Phys. Rev. D* 69(8):082005

Barack L, Sago N. 2007. *Phys. Rev. D* 75(6):064021

Baumgarte TW, Shapiro SL. 1999. *Phys. Rev. D* 59:024007

Baumgarte TW, Shapiro SL. 2003. *Phys. Rep.* 376:41

Begelman MC, Blandford RD, Rees MJ. 1980. *Nature* 287:307–9

Bekenstein JD. 1973. *Ap. J.* 183:657

Bhat NDR, Bailes M, Verbiest JPW. 2008. *Phys. Rev. D* 77(12):124017

Blanchet L. 2006. *Living Rev. Relativ.* 9:4

Blanchet L, Damour T, Iyer BR, Will CM, Wiseman AG. 1995. *Phys. Rev. Lett.* 74:3515–18

Blanchet L, Qusailah MSS, Will CM. 2005. *Ap. J.* 635:508–15

Brink J. 2008. *Phys. Rev. D* 78:102001

Brügmann B, Tichy W, Jansen N. 2004. *Phys. Rev. Lett.* 92(21):211101

Buonanno A, Damour T. 1999. *Phys. Rev. D* 59(8):084006

Buonanno A, Pan Y, Baker JG, Centrella J, Kelly BJ, et al. 2007. *Phys. Rev. D* 76(10):104049

Campanelli M, Lousto CO, Marronetti P, Zlochower Y. 2006. *Phys. Rev. Lett.* 96(11):111101

Campanelli M, Lousto CO, Zlochower Y, Merritt D. 2007. *Phys. Rev. Lett.* 98(23):231102

Carroll SM. 2004. *Spacetime and Geometry: An Introduction to General Relativity*. San Francisco: Addison-Wesley. 1st ed.

Carter B. 1971. *Phys. Rev. Lett.* 26:331

Chernoff DF, Finn LS. 1993. *Ap. J. Lett.* 411:L5

Collins NA, Hughes SA. 2004. *Phys. Rev. D* 69(12):124022

Conway JE, Wrobel JM. 1995. *Ap. J.* 439:98

Cutler C, Flanagan ÉÉ. 1994. *Phys. Rev. D* 49:2658

Damour T. 1983a. In *Gravitational Radiation: Proc. Advanced Study Inst., Les Houches, Haute-Savoie, Fr., June 2-21, 1982*, ed. N Deruelle, T Piran. Amsterdam: North-Holland

Damour T. 1983b. *Phys. Rev. Lett.* 51:1019–21

Damour T. 2008. *Int. J. Mod. Phys. A* 23:1130–148

Damour T, Iyer BR, Sathyaprakash BS. 1998. *Phys. Rev. D* 57:885

Damour T, Nagar A, Hannam M, Husa S, Brügmann B. 2008. *Phys. Rev. D* 78(4):044039

Detweiler S. 2008. *Phys. Rev. D* 77(12):124026

Dewitt BS, Brehme RW. 1960. *Ann. Phys.* 9:220–59

Di Matteo T, Colberg J, Springel V, Hernquist L, Sijacki D. 2008. *Ap. J.* 676:33–53

Dimopoulos S, Graham PW, Hogan JM, Kasevich MA, Rajendran S. 2008. *Phys. Rev. D* 78:122002

Dirac PAM. 1938. *Proc. R. Soc. London Ser. A* 167:148–69

Drasco S, Hughes SA. 2004. *Phys. Rev. D* 69(4):044015

Drasco S, Hughes SA. 2006. *Phys. Rev. D* 73(2):024027

Eddington AS. 1922. *Proc. R. Soc. London Ser. A* 102:268–82

Ehlers J, Rosenblum A, Goldberg JN, Havas P. 1976. *Ap. J. Lett.* 208:L77

Eichler D, Livio M, Piran T, Schramm DN. 1989. *Nature* 340:126

Etienne ZB, Faber JA, Liu YT, Shapiro SL, Taniguchi K, Baumgarte TW. 2008. *Phys. Rev. D* 77(8):084002

Faraoni V. 2007. *Gen. Relativ. Gravity* 39:677

Favata M, Hughes SA, Holz DE. 2004. *Ap. J. Lett.* 607:L5

Ferrarese L. 2002. In *Current High-Energy Emission Around Black Holes*, ed. C-H Lee, H-Y Chang, p. 3. Singapore: World Sci.

Finn LS. 1992. *Phys. Rev. D* 46:5236

Finn LS. 2008. *Phys. Rev. D* 79:22002

Finn LS, Chernoff DF. 1993. *Phys. Rev. D* 47:2198

Fitchett MJ. 1983. *MNRAS* 203:1049–62

Flanagan ÉÉ, Hughes SA. 1998. *Phys. Rev. D* 57:4535

Flanagan ÉÉ, Hughes SA. 2005. *N. J. Phys.* 7:204

Fox DB, Frail DA, Price PA, Kulkarni SR, Berger E, et al. 2005. *Nature* 437:845

Fritschel P. 2003. In *Society of Photo-Optical Instrumentation Engineers (SPIE) Conf. Ser.*, ed. M Cruise, P Saulson, 4856:282. Bellingham, WA: SPIE

Ganz K, Hikida W, Nakano H, Sago N, Tanaka T. 2007. *Prog. Theor. Phys.* 117:1041

Gerke BF, Newman JA, Lotz J, Yan R, Barmby P, et al. 2007. *Ap. J. Lett.* 660:L23

Glampedakis K, Babak S. 2006. *Class. Quantum Gravity* 23:4167

González JA, Sperhake U, Brügmann B, Hannam M, Husa S. 2007. *Phys. Rev. Lett.* 98(9):091101

Haiman Z, Ciotti L, Ostriker JP. 2004. *Ap. J.* 606:763–73

Holz DE, Hughes SA. 2005. *Ap. J.* 629:15

Hopkins PF, Cox TJ, Kereš D, Hernquist L. 2008. *Ap. J. Suppl.* 175:390–422

Hopman C, Alexander T. 2005. *Ap. J.* 629:362–72

Hough J, Rowan S. 2000. *Living Rev. Relativ.* 3:3

Hughes SA. 2000. *Phys. Rev. D* 61(8):084004

Hughes SA, Drasco S, Flanagan ÉÉ, Franklin J. 2005. *Phys. Rev. Lett.* 94:221101

Hulse RA, Taylor JH. 1975. *Ap. J. Lett.* 195:L51

Isaacson RA. 1968. *Phys. Rev.* 166:1272

Jackson JD. 1975. *Classical Electrodynamics*. New York: Wiley. 2nd ed.

Jacoby BA, Cameron PB, Jenet FA, Anderson SB, Murty RN, Kulkarni SR. 2006. *Ap. J. Lett.* 644:L113–16

Kalogera V, Belczynski K, Kim C, O'Shaughnessy R, Willems B. 2007. *Phys. Rep.* 442:75

Kasian L. 2008. In *40 Years of Pulsars: Millisecond Pulsars, Magnetars and More. AIP Conf. Ser.*, ed. C Bassa, Z Wang, A Cumming, VM Kaspi, 983:433. New York: AIP

Kawamura S, Nakamura T, Ando M, Seto N, Tsubono K, et al. 2006. *Class. Quantum Gravity* 23:125

Kennefick D. 2007. *Traveling at the Speed of Thought*. Princeton, NJ: Princeton Univ. Press. 1st ed.

Kim C, Kalogera V, Lorimer DR. 2006. In *Conf. Proc. A Life with Stars—In Honor of Ed van den Heuvel*, Amsterdam, August 22, 2005. In press

Komossa S, Burwitz V, Hasinger G, Predehl P, Kaastra JS, Ikebe Y. 2003. *Ap. J. Lett.* 582:L15

Komossa S, Zhou H, Lu H. 2008. *Ap. J. Lett.* 678:L81

Kormendy J, Gebhardt K. 2001. In *20th Texas Symposium on Relativistic Astrophysics. AIP Conf. Ser.*, ed. JC Wheeler, H Martel, 586:363. New York: AIP

Kramer M, Stairs I. 2008. *Annu. Rev. Astron. Astrophys.* 46:541

Landau LD, Lifshitz EM. 1975. *The Classical Theory of Fields. Course of Theoretical Physics*, Vol. 2. Oxford: Pergamon. 4th rev. Engl. ed.

Lang RN, Hughes SA. 2006. *Phys. Rev. D* 74(12):122001

Leaver EW. 1985. *Proc. R. Soc. London Ser. A* 402:285

Lindblom L, Scheel MA. 2002. *Phys. Rev. D* 66(8):084014

Liu FK, Wu X-B, Cao SL. 2003. *MNRAS* 340:411

Lobanov AP, Roland J. 2005. *Astron. Astrophys.* 431:831

Mackey AD, Wilkinson MI, Davies MB, Gilmore GF. 2008. *MNRAS* 386:65–95

Maness HL, Taylor GB, Zavala RT, Peck AB, Pollack LK. 2004. *Ap. J.* 602:123

McClelland DE. 2002. In *9th Marcel Grossmann Meet.*, ed. VG Gurzadyan, RT Jantzen, R Ruffini, pp. 1864–65. Singapore: World Sci.

Menou K, Haiman Z, Kocsis B. 2008. *N. Astron. Rev.* 51:884–890

Menou K, Haiman Z, Narayanan VK. 2001. *Ap. J.* 558:535–42

Merritt D, Ekers RD. 2002. *Science* 297:1310–13

Merritt D, Milosavljević M. 2005. *Living Rev. Relativ.* 8:8

Mino Y, Sasaki M, Shibata M, Tagoshi H, Tanaka T. 1997. *Prog. Theor. Phys. Suppl.* 128:1

Misner CW, Thorne KS, Wheeler JA. 1973. *Gravitation*. San Francisco: W. H. Freeman

Nagar A, Damour T, Tartaglia A. 2007. *Class. Quantum Gravity* 24:109

Nakar E, Gal-Yam A, Fox DB. 2006. *Ap. J.* 650:281

Narayan R, Piran T, Shemi A. 1991. *Ap. J. Lett.* 379:L17

Nice DJ, Splaver EM, Stairs IH, Löhmer O, Jessner A, et al. 2005. *Ap. J.* 634:1242–49

Nissanke S. 2006. *Phys. Rev. D* 73(12):124002

O'Leary RM, O'Shaughnessy R, Rasio FA. 2007. *Phys. Rev. D* 76(6):061504

Penrose R. 1960. *Ann. Phys.* 10:171

Peters PC. 1964. *Phys. Rev.* 136:1224

Peters PC, Mathews J. 1963. *Phys. Rev.* 131:435

Phinney ES. 1991. *Ap. J. Lett.* 380:L17

Pollney D, Reisswig C, Rezzolla L, Szilágyi B, Ansorg M, et al. 2007. *Phys. Rev. D* 76(12):124002

Portegies Zwart SF, McMillan SLW. 2000. *Ap. J. Lett.* 528:L17

Porter EK, Cornish NJ. 2008. *Phys. Rev. D* 78(6):064005

Postnov KA, Prokhorov ME. 1999. *The 34th Rencontres de Moriond "Gravitational Waves and Experimental Gravity,"* Les Arcs, France, January 23–30, 1999

Pound A, Poisson E, Nickel BG. 2005. *Phys. Rev. D* 72(12):124001

Price RH. 1972a. *Phys. Rev. D* 5:2419

Price RH. 1972b. *Phys Rev. D* 5:2439

Pretorius F. 2005. *Phys. Rev. Lett.* 95(12):121101

Pretorius F. 2007. In *Physics of Relativistic Objects in Compact Binaries: From Birth to Coalescence*, ed. M Colpi, P Casella, V Borini, U Moschella, A Possenti. Astrophys. Space Sci. Libr. Vol. 359. Berlin: Springer

Quinn TC, Wald RM. 1999. *Phys. Rev. D* 60(6):064009

Rathore Y, Blandford RD, Broderick AE. 2005. *MNRAS* 357:834–46

Redmount IH, Rees MJ. 1989. *Comments Astrophys.* 14:165–75

Regge T, Wheeler JA. 1957. *Phys. Rev.* 108:1063

Rezzolla L. 2003. *Summer Sch. Astropart. Phys. Cosmol., July 2002, Trieste.* Int. Cent. Theor. Phys., Trieste, Italy

Robinson DC. 1975. *Phys. Rev. Lett.* 34:905

Rodriguez C, Taylor GB, Zavala RT, Peck AB, Pollack LK, Romani RW. 2006. *Ap. J.* 646:49

Rosswog S, Ramirez-Ruiz E, Hix R. 2009. *Ap. J.* 695:404

Ryan FD. 1995. *Phys. Rev. D* 52:5707

Ryan MP. 1974. *Phys. Rev. D* 10:1736

Sago N, Barack L, Detweiler S. 2008. *Phys. Rev. D* 78:124024

Schmidt W. 2002. *Class. Quantum Gravity* 19:2743

Schnittman JD, Buonanno A. 2007. *Ap. J. Lett.* 662:L63–66

Schutz BF. 1986. *Nature* 323:310

Searle AC, Scott SM, McClelland DE, Finn LS. 2006. *Phys. Rev. D* 73(12):124014

Shapiro SL, Teukolsky SA. 1983. *Black Holes, White Dwarfs, and Neutron Stars: The Physics of Compact Objects*. New York: Wiley-Intersci.

Shibata M, Nakamura T. 1995. *Phys. Rev. D* 52:5428

Shibata M, Uryū K. 2006. *Phys. Rev. D* 74(12):121503

Sigurdsson S, Rees MJ. 1997. *MNRAS* 284:318–26

Spitzer LJ. 1969. *Ap. J. Lett.* 158:139

Stairs IH, Arzoumanian Z, Camilo F, Lyne AG, Nice DJ, et al. 1998. *Ap. J.* 505:352–57

Sundararajan PA. 2008. *Phys. Rev. D* 77(12):124050

Sundararajan PA, Khanna G, Hughes SA, Drasco S. 2008. *Phys. Rev. D* 78(2):024022

Tauris TM, van den Heuvel E. 2003. In *Compact Stellar X-Ray Sources*, Cambridge Astrophys. Ser., No. 39, ed. W Lewin, M van der Klis, p. 623. Cambridge, United Kingdom: Cambridge Univ. Press

Teukolsky SA. 1973. *Ap. J.* 185:635

Thorne KS. 1980. *Rev. Mod. Phys.* 52:299

Thorne KS. 1987. In *300 Years of Gravitation*, ed. SW Hawking, W Israel, pp. 330–458. Cambridge, UK: Cambridge Univ. Press

Thorne KS, Hartle JB. 1985. *Phys. Rev. D* 31:1815–37

Tichy W, Marronetti P. 2007. *Phys. Rev. D* 76(6):061502

Tinto M, Dhurandar SV. 2005. *Living Rev. Relativ.* 8:4

Trias M, Sintes AM. 2008. *Phys. Rev. D* 77(2):024030

Valtonen MJ, Lehto HJ, Nilsson K, Heidt J, Takalo LO, et al. 2008. *Nature* 452:851

Vecchio A. 2004. *Phys. Rev. D* 70(4):042001

Volonteri M, Haardt F, Madau P. 2003. *Ap. J.* 582:559–73

Weisberg JM, Taylor JH. 2005. In *Binary Radio Pulsars. ASP Conf. Ser.*, ed. FA Rasio, IH Stairs, 328:25. San Francisco: ASP

Weinberg S. 1972. *Gravitation and Cosmology: Principles and Applications of the General Theory of Relativity*. New York: Wiley

Yu Q, Tremaine S. 2002. *MNRAS* 335:965–76

Yunes N, Tichy W, Owen BJ, Brügmann B. 2006. *Phys. Rev. D* 74(10):104011

Yungelson L, Portegies Zwart SF. 1997. In *Second Workshop on Gravitational Wave Data Analysis*, ed. M Davier, P Hello, p. 77. Editions Frontieres

Zerilli FJ. 1970. *Phys. Rev. D* 2:2141

Zhou H, Wang T, Zhang X, Dong X, Li C. 2004. *Ap. J. Lett.* 604:L33

Contents

Gamma-Ray Bursts in the *Swift* Era

Indexes

Errata

An online log of corrections to *Annual Review of Astronomy and Astrophysics* articles may be found at http://astro.annualreviews.org/errata.shtml